Chapter 2

Literature review

2.1 Fuel cell electric vehicles

A Fuel cell electric vehicle (FCEV) refers to a vehicle which uses a solid state electrochemical device to convert chemical energy into electrical energy for motor power. The most common fuel source for FCEV's is hydrogen, where energy is produced using oxygen from air and compressed hydrogen stored on board.

A fuel cell is made up from an electrolyte and two electrocatalysts at both the anode and cathode sides of the cell. The electrolyte separates the two electrodes and usually defines the type of fuel cell. At the anode side the fuel is oxidised as shown in equation 2.1, creating a positively charged ion and an electron. The electrolyte is designed to only allow the passage of ions, and prevents the passage of electrons. The freed electron travels through a circuit, creating an electric current to provide power for it's desired use. The ions travel through the electrolyte to the cathode side of the fuel cell where they are reunited with the freed electrons, and oxygen to produce water as shown in equation 2.2. The overall process for a hydrogen fuel cell is shown in equation 2.3 and visualised in figure 2.1

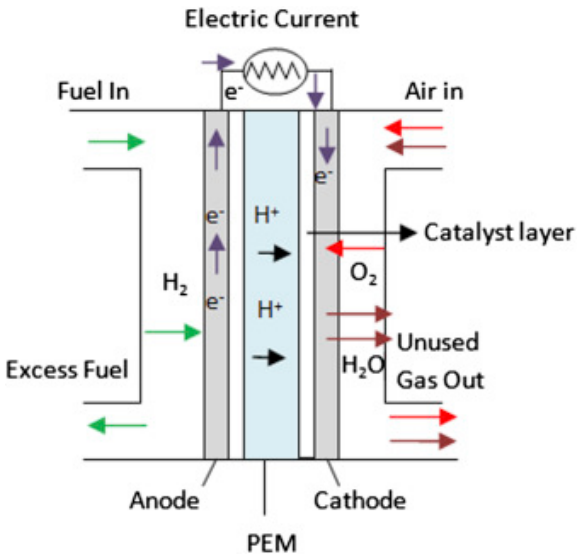

Figure 2.1: Schematic of a PEMFC cell [1]

$$H_2 \rightarrow 2H^+ + 2e^- \tag{2.1}$$

$$\frac{1}{2}O_2 + 2H^+ + 2e^- \rightarrow H_2O \tag{2.2}$$

$$H_2 + \frac{1}{2} \rightarrow H_2O \tag{2.3}$$

While a number of fuel cell technologies can use hydrogen as a fuel source, the most suitable for FCEV's, and in particular mass production of affordable vehicles, are proton exchange membrane fuel cells (PEMFC). This is due to their high power density, low start up time, and low operating temperatures. [2]

A PEMFC uses a proton conducting polymer membrane as an electrolyte material, typically nafion. A PEMFC cell consists of two metal bipolar plates which act to distribute the fuel and oxident within the cell, aid water management within the cell, separate individual cells in a fuel cell stack, and carry current away from the cell. [2] A Membrane electrode assembly (MEA) which consists of the polymer membrane, two dispersed noble metal catalyst layers to enable the anode and cathode reactions, and two gas diffusion layers to ensure uniform access of fuel and oxident to the catalyst layer. Common materials for the MEA are shown in figure 2.2[3]. The components are wedged between two rubber seals to ensure gas the cell is gas tight. Individual cells are combined in series to form a fuel cell stack which can provide the desired power as shown in 2.3

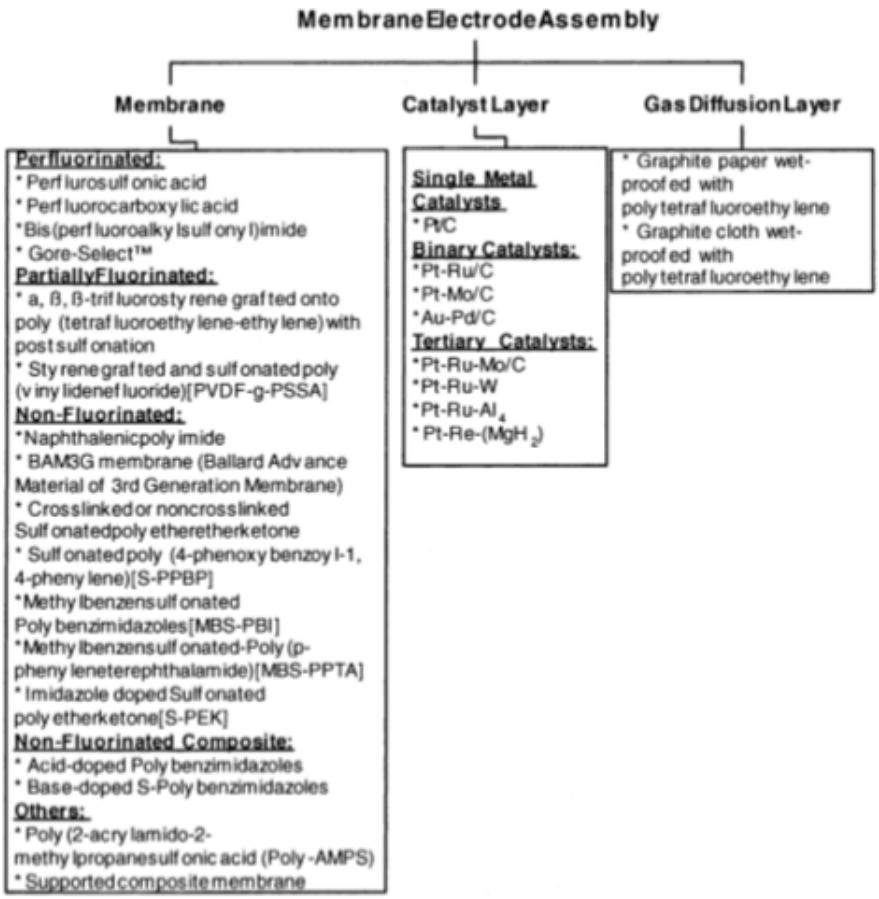

Figure 2.2: Classification of MEA materials [3]

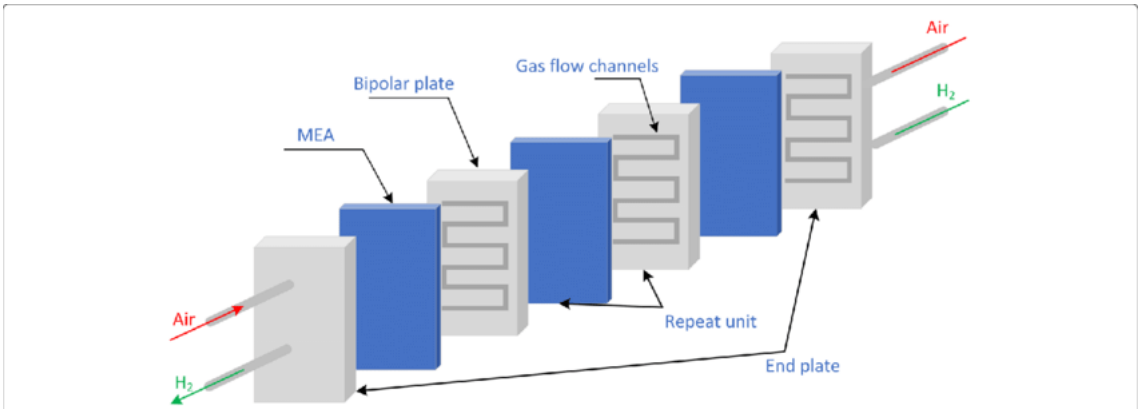

Figure 2.3: Schematic of a PEMFC stack [4]

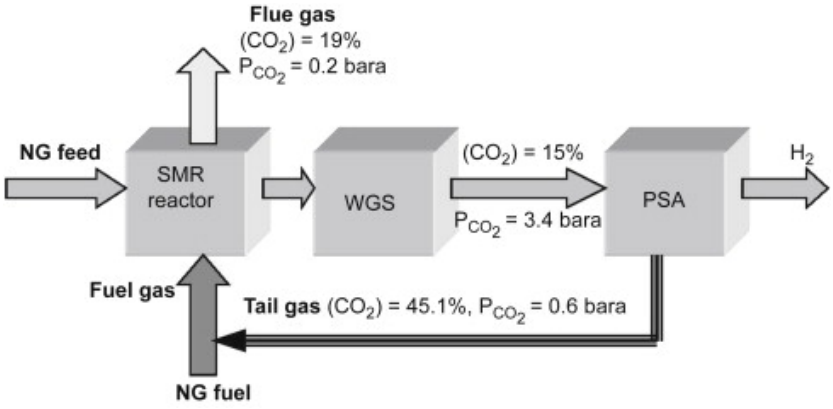

Figure 2.4: Simplified block diagram of a typical modern SMR plant. WGS is a water gas shift reactor. CO_2 concentrations are in mol.%. [8]

2.2 Hydrogen Production

Hydrogen production refers to a range of industrial processes for generating hydrogen. Since there are no natural reserves of hydrogen, it must be obtained through one of these methods. The most important factor for determining the feasibility of a hydrogen production process is the primary source of energy that is used. Currently the options for this are nuclear energy in the form of heat; renewable energy in the form of heat, electricity, light; or fossil fuels either through decomposition of the hydrocarbons present in the fuel, or through heat. Currently the primary sources of hydrogen are from fossil fuels: steam reforming of methane accounts for 48% and other hydrocarbons account for 30% of global hydrogen production; gasification of coal accounts for 18%; and electrolysis of water accounting for the remaining 4%. [5] Electrolysis and SMR will be discussed since these are expected to be the most dominant production methods in the future. [6]

2.2.1 Hydrogen from fossil fuels and hydrocarbons

Fossil fuels are the most dominant source of hydrogen production [5] and there are a number of processes which are commonly utilized in industry. The most popular and therefore the ones which will be discussed are steam methane reforming and hydrocarbon decomposition.

Steam Methane reforming is the conventional and most economical method for producing hydrogen, and it has been predicted by the IEA that this trend will continue despite the emergence of other hydrogen production methods. [7] Steam methane reforming occurs through a two-step chemical process. If another hydrocarbon other than methane is being used it must first be pre-reformed into methane as shown in equation 2.4. A schematic representation of the process can be seen in figure 2.4

$$C_nH_m + H_2O \rightarrow nCO + (\frac{n+m}{2})H_2 \tag{2.4}$$

$$CH_4 + H_2O \rightarrow CO + 3H_2 \quad \Delta H^o_{298K} = +205kJ/mol \tag{2.5}$$

$$CO + H_2O \rightarrow CO_2 + H_2 \quad \Delta H^o_{298K} = -41kJ/mol \tag{2.6}$$

Equation 2.5 takes place in a reactor operating at 700-850°C, at pressures of 3-25 bar, and in the presence of a nickel based catalyst. [8] The result of this step is a mixture of CO and H_2, commonly referred to as syngas. This syngas is further used as a feedstock for the reaction shown in equation 2.6 known as water gas shift in order to produce greater hydrogen yields. This step is carried out in a two-step reaction. An initial high temperature stage at 350°C which converts majority of the syngas to CO_2 and H_2, and a final low-temperature step which operates at 250°C which utilizes a catalyst with higher activity to minimise the remaining CO_2. [8] The final product will be a mixture of CO_2 and H_2.

A number of separation steps are used in order to prevent impurities from contaminating the resulting gas mixture. The traditional separation step is pressure swing adsorption (PSA) which takes advantage of adsorption of gaseous molecules onto a molecular sieve at high pressures. Hydrogen purities of ˜99.9% are achievable using this method however the cost is high and typically contributes to around 20-30% of the total production cost. [8] The other main separation step is desulphurization which uses a combination of CoMo and ZnO catalysts in series at 450-550°C to remove sulphur. [8] This step is essential to ensure sulphur is not present and to ensure catalyst poisoning does not occur at any point in the process.

The cost of producting hydrogen through SMR varies but averages at around £2 per kg of hydrogen and therefore costs around £2000 per tonne of hydrogen produced. [9]

Hydrocarbon decomposition is a process by which hydrocarbon molecules are converted into solid carbon and hydrogen. [10] This reaction is typically operated either thermally or by creating a plasma. A metallic catalyst such as nickel or iron is required. The reaction is shown in equation 2.7 [11]

$$C_xH_2x + 2 \rightarrow xC + (x+1)H_2 \tag{2.7}$$

An advantage of this process is that the only feedstock is the hydrocarbon, so presuming that the feedstock is sufficiently pure this method of hydrogen production should remove the needs for further downstream processing. [10] The main disadvantage of this method is since solid carbon is the main by-product the catalyst will be easily deactivated and will require regular maintenance to ensure carbon build up is managed. [10]

2.2.2 Hydrogen from water

Electrolysis uses an electric current to split water into hydrogen and oxygen using separate anode and cathode chambers isolated using an ion exchange membrane. The anode and cathode reactions are shown in equations 2.8 and 2.9. The main competitive advantage of electrolysis is that reactors are modular and highly scalable, allowing

hydrogen to be produced in a distributed manner. [12] The main input to the process is electricity and if this electricity is produced using renewable sources then the process can be considered carbon neutral. However if a non-renewable source of energy is used the net carbon produced per mole of hydrogen would be higher than that produced by SMR. [13] Electrolysis is incentivised by the increasing price of natural gas and the decreasing price of electricity, which some predict will result in electrolysis becoming more economically feasible than SMR in the future. [12] Currently most commercial electrolysers operate at effieicnies of around 80% and therefore requires around 55000 kWh per tonne of hydrogen produced. The average price of industrial electricity in the UK in 2020 is around £0.13 per kWh [14] and therefore the average price of hydrogen produced through electrolysis is around £7150 per tonne. [9]

$$Anode: \ 2H_2O + 2e^- \rightarrow H_2 + 2OH^- \tag{2.8}$$

$$Cathode: \ 2OH^- \rightarrow \frac{1}{2}O_2 + H_2O + 2e^- \tag{2.9}$$

Thermal decomposition of water is the process of splitting water into hydrogen and oxygen at temperatures of 2000°C as shown in equation 2.10. [6] The operating temperature of the reaction can be lowered under the presence of a nickel or iron based catalyst. [6] Due to the high energy demand for this production method water splitting is not a feasible method of commercial hydrogen production.

$$H_2O \rightarrow H_2 + \frac{1}{2}O_2 \quad \Delta H^o_{298K} = +286kJ/mol \tag{2.10}$$

Chloro Alkali process

The chloro alkali process is an electrolysis process which involves the electrolysis of sodium chloride solutions. The process is already performed on an industrial scale in the production of chlorine and sodium hydroxide. Hydrogen is a by-product of the cathode reaction in the electrolytic cell shown in equation

$$Anode: \ 2NaCl \rightarrow Cl_2 + 2Na^+ + 2e^- \tag{2.11}$$

$$Cathode: \ 2H_2O + 2e^- \rightarrow H_2 + 2NaOH \tag{2.12}$$

$$Overall: \ 2NaCl \rightarrow Cl_2 + 2Na^+ + 2e^- \tag{2.13}$$

It is estimated that around 0.4 million tonnes of hydrogen per year and this could potentially contribute to annual demand. [15] The process is extremely energy intensive however, requiring 2500 kWh per tonne of NaOH produced or 99200 kWh per tonne of H_2 produced. [16] Therefore it is unlikely that this process will be used to solely produce hydrogen. As with many waste gases, producers often reuse the gas to power parts of their process, typically through consumption. It may also be the case that producers

Table 2.1: Summary of ISO 14687-2 impurities in the supply chain and their effects on fuel cell operation adapted from [18]

Impurity	Production sources	Contamination source	Contamination barriers	Effect on fuel cell operation
N_2	SMR	Raw material PSA malfunction	PSA	Reduced energy density of fuel
	Electrolysis	Maintenance Leakage Air intake into water tank	Maintainance PEM membrane H_2 pressure >N_2 pressure supply	
Ar	SMR	Raw materials	PSA	
He	-	-	-	
O_2	Electrolysis	Generation at the anode Membrane cross over TSA malfunction	TSA operating condition Oxygen sensor	Potential damage to hydrogen storage
CO	SMR	By-product Raw materials	PSA CO sensor on line	Temporary electrocatalyst poisoning
CO_2	SMR	By-product Raw materials	PSA	Damage to hydrogen storage medium Could cause formation of CO
	Electrolysis	Water at anodic side Air into the pure water tank	CO_2 filter Anodic separator tank Ion exchange resin in closed water loop PEM membrane	
CH_4	SMR	Raw material	PSA Methane sensor on line	Reduced energy density of fuel
H_2O	SMR	Raw material	PSA	Ice formation during refilling
	Electrolysis	Reactant Through PEM membrane Hydrogen output water saturated TSA malfunction	TSA dryer Dew point monitor Operating procedure	K+ and Na+ contamination reducing cathode side conductivity
Total sulphur compounds	SMR	Raw material	Desulfuration unit Sulphur trap in reforming system PSA	Permanent electrocatalyst poisoning
NH_3	SMR	Raw material	Stainless steel pipe and vessl PSA	Reduced ion exchange capacity
	Electrolysis	Water at anodic side	Reverse osmosis PEM membrane	
Formaldehyde	SMR	Raw material	PSA	Temporary electrocatalyst poisoning
Formic acid	SMR	Raw material	PSA	Temporary electrocatalyst poisoning
Halogenated compounds	SMR	Raw material	Desulfuration unit Chlorinated trap in reforming system PSA	Permanent electrocatalyst poisoning
Monitoring Cl_2 concentration	Electrolysis	Raw material contamination	Stainless steel pipe and vessel Reverse osmosis	

would rather find more efficient methods for performing this rather than selling their hydrogen on the open market. A recent example of this is in 2019 when a chloro alkali plant in Jordan reused their waste hydrogen in a fuel cell situated on site to power their process. [17]

2.3 Hydrogen impurities in the supply chain

The method used to manufacture hydrogen will affect which potential impurities can be present in the final product. While steps are taken in both electrolysis and SMR to ensure a pure product is produced, there is still the chance of impurities reaching the customers fuel cell. This section will explore how ISO 14687-2 impurities can enter the supply chain, and their effect on the operation of a PEMFC. A summary is shown in table 2.1

Water

Water can be present from both SMR and electrolysis due to it being a main by-product of SMR reactions, and the main reactant in electrolysis.

The PSA process used in SMR is an appropriate barrier to prevent water contaminating the end product. This is due to the molecular sieves commonly used having a high selectivity for water. [8] When a PSA system is designed to produce an output of CO below 0.2 µmol/mol, the concentration of water will be less than 0.1 µmol/mol. [18] This makes it unlikely for H_2O to be present in hydrogen produced using this method.

There are three potential pathways for water to contaminate hydrogen through electrolysis. These are:

- Electro-osmosis through the proton exchange membrane
- Hydrogen water saturated at 60°C
- Drier malfunction

Modern electrolysers are fitted with a drier, which is the main barrier for water vapour exiting the process with hydrogen. [18] In the event of drier failure, most systems are fit with a dew point analyser that will trip, shutting off production until the issue can be fixed. [18]

Water can also contaminate produced hydrogen in the chloro alkali process since, similar to electrolysis, it is present in the process. Typically the process contains a drier which ensures that a dew point of -20°C is maintained which should prevent any water in the exit stream.

Water generally does not affect the function of a fuel cell, however; it provides a transport mechanism for water-soluble contaminants such as K^+ and Na^+ [19] to pass through the electrolyte and have a negative long-term effect on the conductivity of the cathode side of the membrane. In addition, water may increase the risk of ice formation within vehicle fuel storage and hydrogen dispensing systems under certain conditions.

Total hydrocarbon content

The presence of hydrocarbons are most likely to result from the SMR process. Hydrocarbons are not expected to be present at all in electrolysis or chloro alkali however could potentially contaminate the system if hydrocarbons are present in any components such as compressors. Similar to water contamination through SMR, the most likely reason for hydrocarbon contamination is due to malfunction of the PSA system used to purify the product hydrogen.

A PSA system designed to deliver hydrogen with a CO concentration <0.2 µmol/mol should be sufficient to reduce the amount fraction of hydrocarbons to below the 5 µmol/mol required by ISO 14687. [18]

Different hydrocarbons have different effects on fuel cell performance. Generally aromatic hydrocarbons adsorb more strongly on the catalyst surface than other hydrocarbons, inhibiting access to hydrogen.[19] Methane (CH_4) is generally considered an

inert constituent and it's main effect on fuel cell performance is diluting the hydrogen fuel stream. [19]

Oxygen

In SMR processes oxygen is not used as a raw material, nor is it stable during the process conditions, readily reacting with hydrogen to produce water. In addition to this the oxygen content of the feedstock to the PSA separation stage must be below a certain level for safety reasons. Therefore oxygen contamination from hydrogen produced from SMR is unlikely.

Oxygen is a main by-product of electrolysis, although is generated at the anode side of the electrolysis stack. Likely methods of contamination are through cross over through the PEM membrane. Due to the danger of high oxygen levels in hydrogen streams, most electrolysis systems are fit with an oxygen sensor that trips the system if the concentration of oxygen in the hydrogen stream surpasses 5 µmol/mol. [18]

Oxygen can also contaminate the exit stream in the chloro alkali process due to it's presence in ambient air. There are no safegaurds in place to prevent oxygen contaminating the hydrogen stream so it is likely that oxygen can be presence in any produced hydrogen if given the opportunity.[18]

Oxygen in low concentrations does not adversely affect the function of the fuel cell system; however, it may be a concern for some on-board vehicle storage systems, for example, by reaction with metal hydride storage materials. [19]

Helium, nitrogen and argon

Helium is not present as a feed material in any of the discussed processes, however there is also no barrier to Helium in the exit stream and therefore any helium that enters a SMR or electrolysis process will not be removed. Despite this it is unlikely that helium will be present in a hydrocarbon feedstock, or water.

Argon is similar to helium, however it is more likely for Argon to be present in the natural gas feedstock for SMR. Unlike helium, the PSA step in SMR can act as a barrier for Argon, however this will depend on the specific molecular sieve used in the system. [18]

Nitrogen is the most likely inert impurity to be present in fuel cell hydrogen, this is due to the abundance of nitrogen in the air which the system could be exposed to, and the frequency at which nitrogen is used as a functional gas in processes for purging chambers, actuating valves etc.

Inert constituents, such as helium (He), nitrogen (N_2) and argon (Ar) do not adversely affect the function of fuel cell components or a fuel cell system. However, they dilute the hydrogen gas. N_2 and Ar especially can affect system operation and efficiency and can also affect the accuracy of mass metering instruments used for hydrogen dispensing. [19]

Carbon dioxide

Like most other impurities which are present in SMR, CO_2 is likely to be removed from the SMR process at the PSA step, with most commonly used molecular sieves being able to remove carbon dioxide during normal operation. [8]

CO_2 can be present in the water used for electrolysis although there are several interlocks to prevent it reaching the exit stream. Most electrolysis systems have a CO_2 filter on the inlet and a reverse osmosis unit to ensure the purity of the inlet water. An anodic separation tank which features an ion exchange resin in a closed water loop also acts as an additional barrier, and finally CO_2 has a low crossover potential through the PEM membrane and therefore is unlikely to cross into the cathode side of the system.[18]

Carbon dioxide is not likely to be in the product stream from hydrogen produced in chloro alkali as is remains in the caustic soda lye that is produced. CO_2 could also be formed from oxidation of the membrane material when degraded however no quantitative assesment has been made on this. [18]

CO_2 does not typically affect the function of fuel cells. However, CO_2 may adversely effect on board hydrogen storage systems using metal hydride alloys. With CO_2, at levels higher than the specification, a reverse water gas shift reaction can occur under certain conditions in fuel cell systems to create carbon monoxide. [19]

Carbon monoxide

Carbon monoxide is a main byproduct of SMR which is separated from the exit gas stream through PSA. [8] If this fails SMR processes are fitted with a CO sensor to ensure the concentration in the product does not pass a certain threashold. [18] It is unlikely for CO to be present from electrolysis.

Carbon monoxide (CO) is a severe catalyst poison that adversely effects fuel cell performance by inducing a competitive adsorption effect between itself and hydrogen on the electrocatalyst surface. The result is a temporary reduction in operating efficiency. [19] Although its effect can be reversed through mitigating strategies, such as material selection of membrane electrode assembly (MEA), system design, and operating conditions, it's effect on operation is still a concern. Lower catalyst loadings are particularly susceptible to catalyst poisoning contaminants.

Total sulfur compounds

Sulphur contamination is most likely to come from hydrogen produced from hydrocarbon sources. Since the SMR process also uses catalysts that are susceptible to poisoning from sulphur compounds all plants are fit with a desulphurisation unit upstream from the main process. [8] This is designed to reduce the concentration of sulphurous compounds to $<$50 nmol/mol. [18]

Should the desulphurisation unit fail the catalysts used in both reforming steps will be deactivated, preventing the process from operating and will likely result in shut down

of the plant. PSA also acts as a final barrier, since H_2S will adsorb onto the molecular sieves more strongly than CO. [18]

The other potential source of sulphur contamination is the potential release from any gasket materials used in the process. This can be easily prevented by ensuring only materials that do not contain sulphur are used. [19]. It is unlikely that sulphur contamination will arise from electrolysis.

Sulfur containing compounds are severe catalyst poisons that at even very low levels can cause irreversible degradation of fuel cell performance due to a permanant reaction taking place between sulphur and the platinum catalyst. The specific sulfur compounds addressed in particular are: hydrogen sulfide (H_2S), carbonyl sulfide (COS), carbon disulfide(CS_2), methyl mercaptan (CH_3SH). [19]

Formaldehyde and formic acid

Formaldehyde (HCHO) and formic acid (HCOOH) is a produced through a side reaction in SMR depending on the specific operating conditions of the process.[8] PSA is the main barrier for preventing contamination of the product. [18]

Formaldehyde and formic acid have a similar effect on fuel cell performance as CO and are thus considered as reversible contaminants. The effect of HCHO and HCOOH on fuel cell performance can be more severe than that of CO due to slower recovery kinetics and their specifications are lower than that for CO. [19] Lower catalyst loadings are particularly susceptible to catalyst poisoning contaminants.

Ammonia

Hydrogen could be contaminated with ammonia through either SMR or electrolysis. Ammonia is a by-product of the reforming steps and PSA should be sufficient to remove ammoinia from the exit stream of SMR. Ammonia can also be present in water used in electrolysis however the reverse osmosis step used to purify the water before the process is normally sufficient in removing all ammonia before it is used in the process. [18]

Ammonia (NH_3) causes some irreversible fuel cell performance degradation by affecting the ion exchange capacity of the ionomer of the proton exchange membrane. [19]

Total halogenated compounds

Halogenated compounds can contaminate hydrogen by entering either SMR or electrolysis through the process input, or leaking into the process at other points where they are used. Potential sources include chlor-alkali production processes, refrigerants used in processing, and cleaning agents. [18]

In the chlor-alkali process, the presence of chlorine and hydrochloric acid in hydrogen gas could be likely since they are main feedstocks in the process. Both HCl and Cl_2 are highly soluble in water and are likely to leave the process in solution. Cl_2 and H_2 are also contained separatley from each other and not expected to cross contaminate.

Cross contamination could occur in the event that there is not enough liquid water in the system. This would likely be detected as the system would quickly fill with hydrogen gas which is continuously monitored due to risk of explosion, shutting down the system and preventing contaminated hydrogen leaving. Therefore it is unlikely that Cl will be present in the produced hydrogen. Halogenated compounds cause irreversible performance degradation similar to sulphur, reacting with the platinum electrocatalysts to form platinum-halides such as $PtCl_4$. [20] However the concentrations required to cause this damage has not been well documented in literature.

Other impurities

2.4 Hydrogen impurity enrichment

'Hydrogen impurity enrichment' is a term for any technique which involves increasing the concentration of impurities within a hydrogen sample by means of removing the hydrogen matrix gas. There are two previous reports of impurity enrichment being used as a technique for hydrogen impurity analysis. The first report by Papadis et al at Argonne National Laboratory used a Pd/Cu [21] coated Pd/Ag membrane for non-sulphur containing hydrogen samples and a Pd/Au coated Pd/Ag membrane for sulphur containing hydrogen samples to enrich impurities in a 50 bar sample. The analyte gas used contained N_2, CH_4 and CO_2 at 100µmol/mol and an additional 2 µmol/mol of H_2S during sulphur tests sulphur. The enrichment was calculated by using measured values of temperature and pressure along with the non-ideal gas law, this was represented through a 'calculated enrichment factor' as shown in equations 3.1 and 2.15.

$$CEF_{NI} = \frac{\frac{P_{1,a}V_1}{Z_{1,a}RT_{1,a}}\frac{P_{2,a}V_2}{Z_{2,a}RT_{2,a}} - \frac{P_{1,b}V_1}{Z_{1,b}RT_{1,b}}}{\frac{P_{2,b}V_2}{Z_{2,b}RT_{2,b}}} \tag{2.14}$$

$$y_{i,a} = \frac{y_{i,b}}{CEF} \tag{2.15}$$

The set-up was able to reach enrichment factors of around 32 for non-sulphur tests and 15 for sulphur tests. The non-sulphur tests closely matched with the actual component concentrations, however in the second set of tests there was some loss of sulphur observed, most likely due to the formation of palladium sulphide on the surface of the membrane, or through wall catalysed reactions.

A similar experiment was performed by National Physical Laboratory with the aim of decreasing the uncertainty of using such a device. [22] The non-ideal gas law method used in the previous paper [21] was compared to a novel tracer enrichment method developed by NPL. [22] The tracer enrichment method involves spiking the hydrogen sample with a known quantity of krypton prior to enrichment. The enrichment factor is then calculated using the change in concentration of the krypton as shown in equation 2.16.

$$CEF_{Tracer} = \frac{y_{kr_b}}{y_{Kr_b}} = \frac{1}{y_{Kr_a}} \frac{A_{Kr_b}}{A_{Kr_a}} y_{Kr_{st}} \tag{2.16}$$

The set-up was similar to the one used by Papadias et al [21] and was used to enrich a 50 bar 10L hydrogen sample containing 1.5-2 µmol/mol of CO, Kr, CH_4 and N_2. Use of the tracer enrichment method reduced the associated uncertainty from 2.6% to 1%. Two tests were performed, with the second test resulting in membrane failure.

When operating the hydrogen impurity enrichment device it was found that both methods should be used to calculate the CEF.[22, 23] While the tracer enrichment method has a lower uncertainty due to it being dependant on fewer variables, it is impossible to tell if a leak has occurred in the device due to the covariance phenomena. [22] Leaks in the enrichment device could occur due to thermal expansion of components due to heating to the required operating temperature or cracks forming in the membrane. The stability of membranes used in such a device will be discussed in the following section. During a leak it will be expected that the ratio of krypton, along with other impurities which are not naturally present in air, will remain constant, resulting in no change in the CEF. A leak will allow oxygen and nitrogen to enter the system and throw off the measurement of these two impurities. While the tracer enrichment method could still be used to calculate the amount fraction of other impurities, the non-ideal gas law method would have to be used to provide an accurate measurement for Oxygen and Nitrogen.

A device similar to the HIED is the Hydrogen Elimination Mass Spectrometer (HEMS) designed by Power + Energy USA. [24] The principle behind the HEMS is the same as the HIED, where a palladium membrane is used to selectively remove the hydrogen matrix gas and thus concentrate the impurities within the hydrogen sample. The output is directly fed into a mass spectrometer which allows in-situ measurements to be performed. The limit of detection specified by the manufacturer claims to be in the range of pmol/mol however there is no published information regarding the accuracy or uncertainty associated with the device. As of 2016 the device was discontinued by the manufacturer.

2.4.1 Other enrichment methods

Sorbent tubes

The use of traps and sorbent tubes to pre-concentrate impurities in gases is very common in gas analysis, but only two hydrogen purity analysis standards have incorporated this technique to facilitate purity analysis. A method for concentrating the impurities in a sample of hydrogen using a zeolite- packed chromatographic column has been described in a paper by Hille [25]. The method involves flowing the gas sample into the column using a pump and cooling the column to a temperature that allows the impurities to remain trapped whilst the matrix gas passes through. The sample is then transferred to GC-MS for analysis. The enrichment factor for this method is determined by the flowrate and amount of time that the gas is sampled into the column. The method

was validated by analysing gas mixtures of hydrogen containing 8.7 mmol/mol of silane. By enriching the sample, the signal- to-noise for the same measurement was increased by a factor of 2000 indicating that levels in the range of 4 nmol/mol of silane would easily be measured using this method whereas the usual limit of detection (without pre-concentration) would have been 1 µmol/mol

Cryo-focusing

A method for performing pre-concentration by cryo-focusing has been detailed in ASTM WK34574 where the device is used to concentrate the impurities in a sample of hydrogen before introducing the gas to a GC-MS [23] The pre-concentration method involves trapping the impurities onto a glass bead trap at -150°C. By increasing the temperature of the trap all of the impurities apart from water are transferred to a separate Tenax trap which is cooled to -170°C. Upon heating once again the enriched sample is introduced to the analyser. Very high enrichment factors can be achieved using this method by flowing a high volume of the sample gas through the pre-concentration device to allow capture of the impurities whilst the hydrogen is removed. No information was provided in the standard to indicate the accuracy or limitations of this method.

2.5 Review of hydrogen selective membranes

The term membrane is used to describe a semipermeable barrier which selectively allows certain species to pass through it, while preventing or inhibiting the passage of others. The driving force for gas separation through a membrane is the pressure and component concentration gradients across the chosen material. In the context of hydrogen separation, the trans-membrane pressure and hydrogen concentration gradient across the feed and permeate, combined with the unique properties of the chosen separation material, will allow hydrogen to pass through the membrane, while preventing or inhibiting the transport of impurities which the membrane is not selective or less selective towards. A large number of materials have been studied for hydrogen separation. For the purpose of this review they will be split into four broad categories based on their material type and separation mechanism which is related to their pore structure (dense or porous); these categories are shown in Table 2.2 and visualized in Figure 5.1.

The material, its structure with regards to pore size and pore size distribution, and surface chemistry, all contribute to the separation mechanism for removing hydrogen from its constituent gas mixture. The six main membrane separation mechanisms are visualised in Figure 5.1, with (i) – (iv) showing the four separation mechanisms for gases in porous media, and (V)- (Vi) showing gas separation through dense media. For porous materials typically a combination of these mechanisms dictates the overall separation performance due to imperfections in the membranes structure. All dense membranes should be dictated by the solution diffusion mechanism and the presence of any other mechanisms are evidence of imperfections in the membrane.

For most porous media, the separation mechanism is dominated by Poiseuille flow or

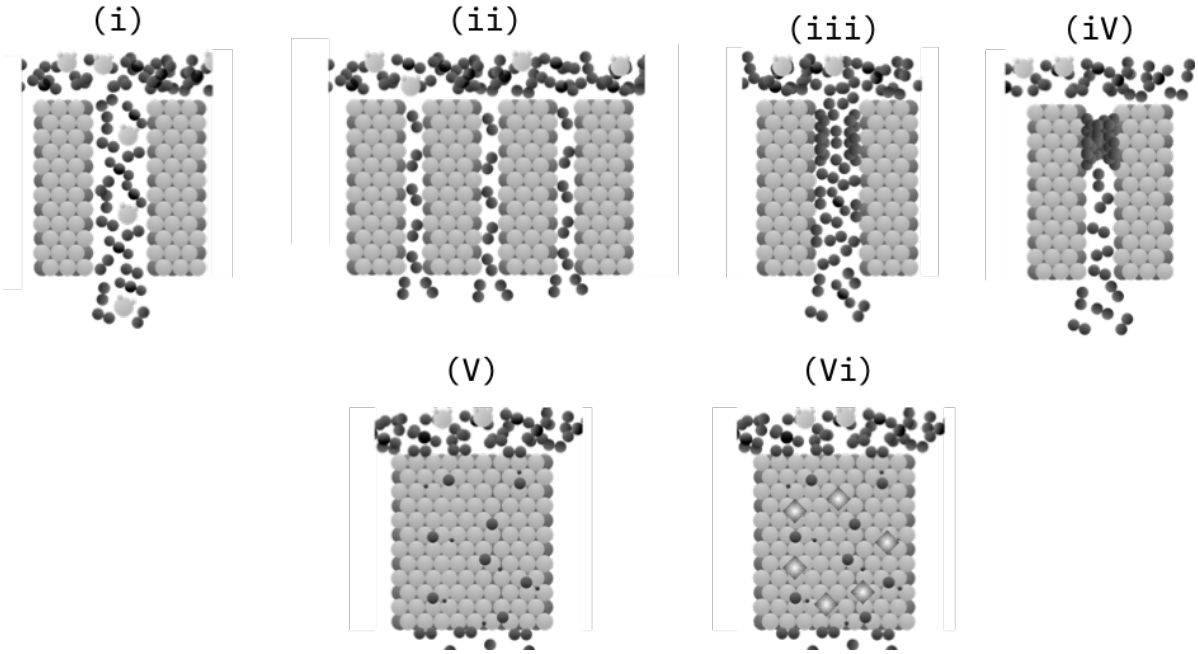

Figure 2.5: Illustration of the five membrane separation mechanisms (i) Poiseuille Flow/Knudsen diffusion, (ii) Molecular Sieving, (iii) Surface diffusion (iV) Capillary condensation (V) Solution diffusion (Vi) Facilitated transport

Knudsen Diffusion. The precise separation mechanism can be determined by calculating the ratio between the mean free path of the gas molecules (λ) and the pore radius (r) as shown in Equation 2.17 where η is the viscosity of the gas, P is the pressure, T is the temperature, M_w is the molecular weight of the gas, and R is the universal gas constant.

$$\frac{r}{\lambda} = \frac{2P}{3\eta}\sqrt{\left(\frac{2M_w}{\pi RT}\right)} \tag{2.17}$$

This ratio determines the contribution of Knudsen and Poiseuille flow. If $r/\lambda > 1$ it would indicate that the main gas transport rate limiting step is due to molecule-molecule collisions indicating that Poiseuille flow is the dominant transport mechanism. Likewise if $r/\lambda < 1$ it indicates that molecule-wall collisions govern the rate limiting step showing that Knudsen diffusion is the dominant mechanism. If the transport is purely Knudsen diffusion the H_2/CO_2 selectivity of the membrane will be equal to around 4.7. Since this value is relatively low, it has pushed researchers into fabricating membranes with smaller pore structures, and to modify their membranes to take advantage of specific surface interactions. Both of these developments allow researchers to surpass the selectivity achievable with purely Knudsen diffusion.

Molecular sieve materials can be classed as macroporous (>50nm), mesoporous (2-50nm) and microporous (<2nm) with microporous materials being the most relevant for hydrogen separation processes. These membranes are fabricated in such a way that the passageways are small enough that the entrance of molecules with large kinetic

diameters is not possible. This results in higher permeation of smaller components in a gas mixture such as H_2 or He while slowing, or completely preventing the passage of bulkier molecules. This mechanism, while effective for some gas mixtures, may not be feasible when looking to perform separation on similar sized gas pairs; selectivity is often hindered by competitive adsorption between the species due to the surface chemistry of the material. Fabrication of these membranes can also be difficult and manufacturing large scale membranes with a tight enough pore size distribution to ensure molecular sieving still proves to be a difficult task. Common microporous materials which are able to be fabricated into molecular sieving membranes are zeolites, metal organic frameworks, activated carbon, and amorphous silica.

Surface diffusion and capillary condensation are similar in that the surface chemistry of the pores in the membrane has a large effect on the separation efficiency. Surface diffusion occurs when the walls of the pore either intrinsically, or following modification, provides adsorption sites for the desired gas molecule. The gas molecule will adsorb onto the walls resulting in faster diffusion through the pore structure than other gases in the mixture. Similarly, capillary condensation typically follows on from surface diffusion and involves the gas species condensing within the pore of the membrane, either due to stronger molecule-wall interactions, or a smaller pore radius. The condensation of the molecule results in further selectivity improvements towards this component by providing an added transport barrier to other gas species.

Gas transport in dense media is typically harder to categorise due to the unique material chemistry present in each material, however all dense membranes perform separation through some variation of the solution diffusion mechanism. Typically, the following steps are always present in some form:

1. Adsorption of gas species onto the surface of the membrane
2. Diffusion of gas species through the bulk of the membrane
3. Desorption and diffusion of the gas species in the downstream.

More details will be provided on the precise features of solution diffusion in each material in the following sections. Facilitated transport is a sub section of solution diffusion and occurs in dense membranes which have a selected chemical species added into the bulk of the membrane. These materials are chosen based on the presence of a particular interaction with components of a gas species. These interactions are typically reversible reactions between the added species and the gas intended for separation and is intended to enhance the diffusion of the selected gas, this additive could either be fixed species (solid) or mobile (liquid).

The most commonly reported metrics for membrane performance is the flux or permeability coefficient and selectivity. The flux (J) of a membrane is a measure of the amount of gas the membrane is allowing to pass per unit time per unit surface area and is typically used as a measure for how effective the fabricated membrane performs. The permeability coefficient (P) can be derived from the flux and is a quantitative expression which gives a specific measure of the separation properties of a material independent

of operational and manufacturing constraints such as operating pressure and membrane thickness. While flux and permeability are similar and tied to each other they are both useful in their own way. The permeability coefficient is typically tied to the material and is useful for comparing different materials to each other, while the flux offers a measure on how effective a specific membrane is.

The selectivity ($\alpha_{i/j}$) represents the separating ability of the membrane for a specific gas species (i) with respect to another gas species (j). This is common notation for porous membranes and membranes which are not completely selective towards one component. For membranes which are only selective towards one component such as dense metal and dense ceramic, the selectivity is not reported since any presence of another component in the exit stream is generally an indication of a manufacturing defect.

While these values are reported for all membranes in order to allow for a direct comparison of performance, this is where the similarities end. The fundamental separation mechanism, manufacturing techniques, and unique material chemistry are often different for each material. In addition to this there are other important metrics for the usefulness of a membrane such as mechanical stability, lifespan, and chemical resistance which are more difficult to quantify.

Table 2.2: Types of hydrogen separation membrane

Material	**Separation mechanism**	**Mechanical stability**	**Chemical Stability**	**Operating temperature**	**Selectivity**
Polymer (Dense)	Solution diffusion, Facilitated transport	Susceptible to Compaction [26] and Swelling [27]	Low chemical stability, Degrades under H_2S, HCl, CO_2, SO_x [28]	$< 100^{O}C$	2.5 [29] – 960 [30]
Nano-porous	Knudsen diffusion, Poiseuille flow, Capillary condensation, Surface diffusion, Molecular sieving	Brittle	Good[31]	Ambient -500°C	2.4 [32] - 1000 [31] (H_2/N_2 selectivity)
Dense Metal	Solution Diffusion	Phase transition [33] Dependant on support [33] Surface segregation[33]	Negative interaction with CO, CH_4, and H_2O. Reacts with H_2S and SO_x [33]	300-600 [34]	∞
Dense Ceramic	Solution Diffusion	Brittle Difficult to seal due to high operating temperature	Degrades under CO_2 [35]	500-1000 [35]	∞

2.5.1 Criteria for a hydrogen impurity enrichment material

In order for a membrane to be suitable for hydrogen impurity enrichment material it must be able to increase the concentration of low-level impurities in a hydrogen sample. Although all past examples of hydrogen impurity enrichment have used dense membranes with an infinite selectivity towards hydrogen, it is theoretically possible to use a membrane which has a lower selectivity to perform enrichment. This would have the advantage of allowing membranes with faster flux to be used, greatly reducing the amount of time required for an enrichment run, while allowing cheaper materials to be used in place of the palladium membranes used in past studies. In order to perform this calculation, the following must be known:

- Selectivity of the membrane must be known to a high accuracy
- Total number of moles leaving the system
- Concentration of enriched impurities

Since the selectivity shows the ratio of substances passing through the membrane (i.e. H_2/N_2 selectivity of 2 represents 2 moles of hydrogen for every 1 mole of nitrogen passing through the membrane) if both quantities are known the number of moles of impurity leaving the system through permeation could be easily estimated.

$$n_{i_{exit}} = n_{exit_{total}}/\alpha^{H_2/i} \tag{2.18}$$

The concentration, and therefore the number of moles of impurity on the retentate side of the membrane could then be analysed using suitable instrumentation. These values could then be added together and divided by the enrichment factor in order to give the original number of moles that would be in the vessel.

$$y_i = \frac{(n_{i_{ret}} + n_{i_{exit}})/n_{tot_{ret}}}{CEF} \tag{2.19}$$

In practice however this may not be feasible due to the low concentrations of impurities expected to be present in these hydrogen samples. In order for an enrichment calculation to work there must be an analysable concentration of impurity remaining in order to back calculate. Since the level of expected impurities in a hydrogen sample is so low, and the selectivity of many membranes also low, there is a high risk of either all impurities simply leaving the sample during the enrichment run, or only achieving a lower enrichment factor. Take the example of enriching a sample containing 0.2 µmol/mol of CO by 100 in order to analyse its composition on a GC-MS. If the sample is a standard 10L cylinder containing 100 bar a H_2/CO selectivity of ˜4950000 is required to simply prevent all of the CO leaving the enrichment device, which is effectively the same as the selectivity's seen in dense metal membranes. However, for the same sample containing 0.3 µmol/mol of Helium a H_2/He selectivity of 330 is the minimum required which is more feasible. However, both these values are the exact values required by the standard, in reality they would be much lower. The highest reported selectivity of a

non-infinitely selective membrane was Liquid crystalline polyester which had a H_2/N_2 selectivity of 2632 [36] which indicates that this method may be suitable for enriching some of the higher concentration impurities in hydrogen samples, it is not a solution for lower concentration. It is also unlikely that the selectivity of a membrane material will stay constant throughout its lifespan. Any drift in selectivity would throw off the calculation and either require regular changing of the membrane, driving up cost, or regular calibration to recalculate the selectivity of the membrane at a given time, which would be time consuming. It is however likely that infinitely selective membranes are the only feasible enrichment material due to their ability to enrich every impurity in hydrogen, whereas non-infinitely selective membranes may be applied to analysis of individual impurities, it is unlikely such a scenario would occur in reality which makes them a non-ideal solution.

The common thread with all the micro-porous materials discussed here is that they are currently difficult and expensive to synthesise on a large scale, particularly in membrane form. Due to the separation mechanism of micro-porous materials they are not suitable for use in hydrogen impurity enrichment as their selectivity will not produce a viable enrichment medium. However, due to their high surface areas and ability to be modified to promote integration with specific gas species, they may find use in sensor applications for detecting the ISO-14687 impurities. There is a wealth of work on the use of many of these materials as chemical sensors however much of this work has been performed using the gases in non-hydrogen matrix gases and therefore much work is required before their true potential in this area can be realised.

Polymer membranes have a similar issue to micro porous materials in that their selectivity is too low to be effective at enriching impurities in hydrogen samples. The mechanical strength and impurity resistance of polymer membranes also limits their use as hydrogen impurity enrichment mediums. While again there are some successful applications of polymers as sensor materials, the same issues as micro porous materials regarding lack of information of their effectiveness in a hydrogen matrix crops up again. It is likely that polymer membranes will continue to be most effective in industrial separation and will be limited in their use as an analytical material.

Therefore this section will only concern itself with membranes which show permaselectivity towards hydrogen therefore making them viable as hydrogen impurity enrichment materials. This section will discuss the performance of dense metallic and dense ceramic membranes, and by comparing their reported metrics, their suitability for hydrogen impurity enrichment will be determined.

Dense metallic

Metallic membranes are comprised of dense metal or alloy sheets which allow the permeation of hydrogen through its constituent electrons and protons. While this is the same separation mechanism seen in dense polymer membranes the hydrogen selectivity is typically a lot higher in these systems since molecules which are not hydrogen are unable to dissociate and permeate through the membrane surface, giving a theoretically infinite selectivity towards hydrogen. The minimum requirement for a dense metal mem-

brane for hydrogen separation is the ability to dissociate and permeate hydrogen. There are a number of metals which have shown varying degrees of suitability for hydrogen separation and these are shown in Table 2.3.

Table 2.3: Metals which show the ability for hydrogen permeation [37]

Structure	Metal	Activation energy for hydrogen permeation (kJ/mol)	Heat of hydride formation (kJ/mol)	Hydrogen permeability at 500°C (mol/ m s $pa^{1/2}$)
fcc	Ni	40.0	-6	7.8×10^{-11}
	Cu	38.9	-	4.9×10^{-12}
	Pd	24.0	20	1.9×10^{-8}
	Pt	24.7	26	2.0×10^{-12}
bcc	V	5.6	-54	1.9×10^{-7}
	Fe	44.8	14	1.8×10^{-10}
	Nb	10.2	-60	1.6×10^{-6}
	Ta	14.5	-78	1.3×10^{-7}

The flux of a dense metal membrane is given by Eqn 2.20 and is a function of the metals permeability to hydrogen, the concentration and pressure gradient across the membrane, and the thickness of the dense layer.

$$J = \frac{\phi}{l}(P_{H,ret}^{0.5} - P_{H,perm}^{0.5}) \tag{2.20}$$

From the metals shown in Table 2.3 palladium and its alloys are by far the most popular choice due to a combination of high hydrogen permeability, favourable catalytic activity towards hydrogen dissociation and re-association, and aversion towards hydride formation compared to other metals.[37, 38, 39]

For other metals there is often a trade-off, V, Nb and Ta exhibit higher permeability than palladium but are limited by their low catalytic activity for hydrogen dissociation and typically must be combined with another metal to compensate for this. A common strategy is to deposit palladium particles on both sides of membranes made from these metals to provide this catalytic activity. Embrittlement of pure metal membranes is also an issue, even for metals with a high heat of hydride formation. Embrittlement is a side effect of hydrogen passing through the crystal lattice. During transport a H-M phase will form which has a higher lattice parameter than the original crystal lattice. This change in lattice parameter can cause stress in the overall structure of the dense membrane layer and cause the formation of pin holes, cracks, and eventually membrane failure. Metals with a low heat of hydride formation in Table 2.3 will readily embrittle within hydrogen containing atmospheres.

This section will discuss developments in both palladium and non-palladium membranes and the issues still surrounding the technology.

As previously mentioned palladium is typically the material of choice for dense metallic membranes due to its combination of high stability, permeability, and catalytic activity. Palladium based membranes have been successfully used to provide ultrapure hydrogen for a number of applications including electronics, industrial gas, and fuel cell

industries for a number of years. The main downside to the use of palladium is its high cost of around $25 per gram. [40] This high cost has pushed researchers into focusing on reducing the amount of palladium used in the membrane in order to find a more economical solution. This is done either by using a traditional membrane approach, whereby the thickness of the membrane layer is reduced as much as possible to maximise the flux while decreasing the overall amount of palladium used, or by alloying palladium with a cheaper metal to reduce the amount of bulk palladium in the manufacturing process.

During operation of a pure palladium membrane at temperatures lower than 300°C, hydrogen embrittlement can occur due to the aforementioned phase transition between interstitial hydrogen within palladium (α phase) and palladium hydride (β phase). The β phase (0.4025 nm) has a lattice parameter bigger than the α phase (0.389nm). [41] The formation of this α - β phase will cause the membrane to distort, become brittle, and eventually results in membrane failure when a leak occurs. [42] The behaviour of hydrogen embrittlement is shown in figure 2.6 Aside from this pure palladium has poor chemical stability, it can be poisoned by a number of impurities which are commonly found in hydrogen. Some of these impurities simply inhibit permeation of hydrogen but do not have a permanent interaction and thus their effects can be mitigated by optimising the operating conditions. Others such as H_2S and CH_4 are known to interact with the membrane through chemisorption and permanently damage the membrane through the formation of compounds with palladium, breaking the crystalline lattice resulting in membrane failure.

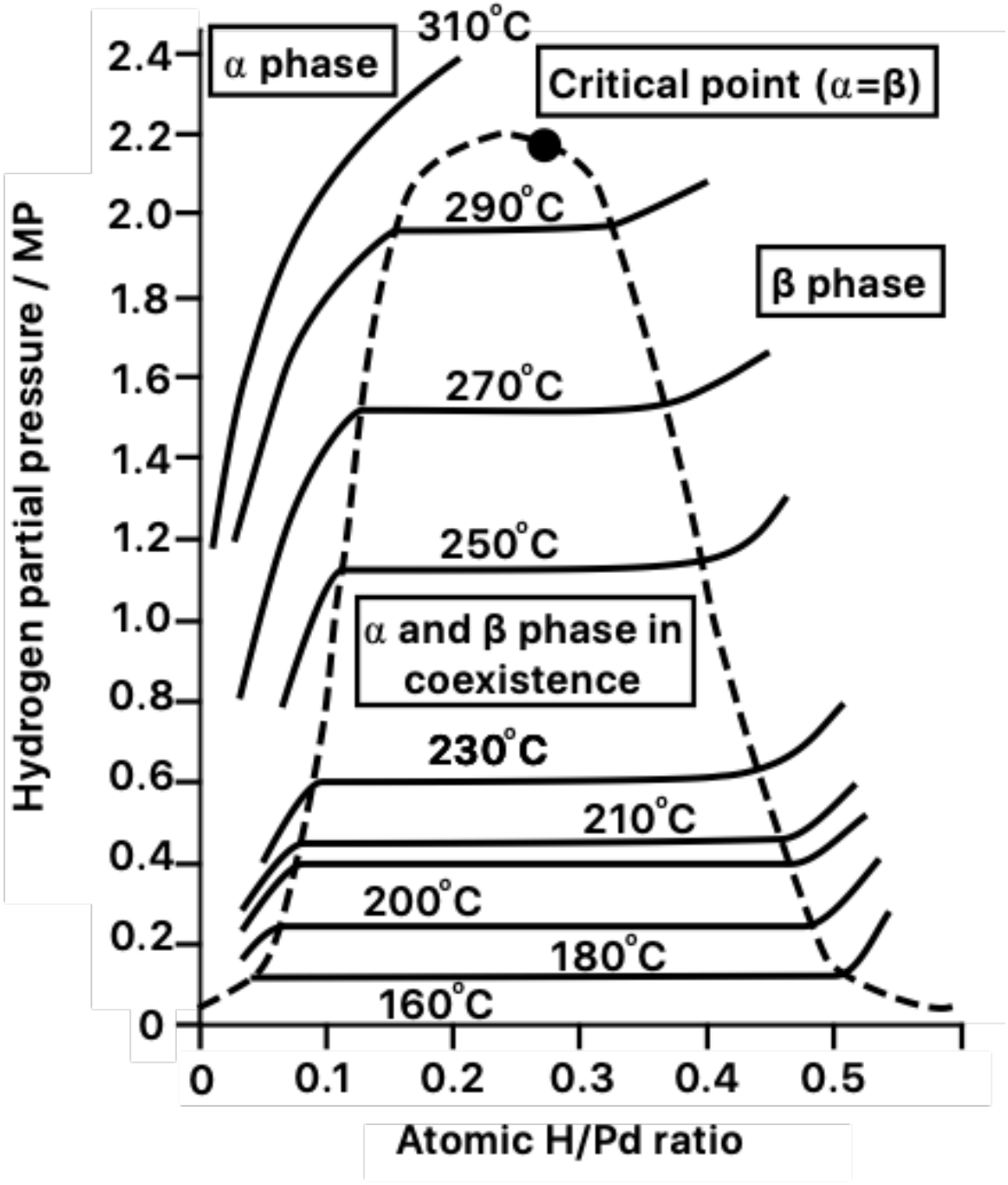

Figure 2.6: Palladium-Hydrogen phase diagram adapted from [42]

From the impurities listed in ISO 14687-2 CO, H_2O, Hydrocarbons and sulphur containing compounds are known to have a physisorption interaction with palladium. Physisorption based poisoning occurs by the impurity inducing a competitive adsorption with hydrogen, blocking active sites for hydrogen dissociation, and hence reducing the active area available for hydrogen permeation.[33] The ultimate effect of this is a

temporary flux reduction which has no long lasting damage on the membrane. Compounds such as H_2S have a more extreme effect on the membrane as adsorption leads to a reaction between palladium and the metal permanently changing the membrane composition and structure. The most commonly studied interaction is the interaction between palladium and H_2S to form palladium sulphide. Palladium sulphide, while still permeable to hydrogen, has an extremely low permeability, drastically reducing the efficiency of the membrane. Palladium sulphide also has a larger lattice constant than that of pure palladium which can lead to membrane failure by creating gaps in the crystal lattice resulting in pinholes. Some of these impurities, in particular those which only exhibit physisorption, can be mitigated by altering the operating conditions. It has been reported that the effects of CO and H_2O poisoning can be completely eliminated by operating at temperatures above 300°C. Another example where this is shown is with H_2S related poisoning. Since the reaction between palladium and H_2S is exothermic, and produces hydrogen as a side product, it can be inhibited by increasing the H_2:H_2S ratio and increasing the temperature.

A combination of cost, easy formation of phase transitions [41, 42] and its low tolerance for common impurities found in hydrogen processes limits pure palladiums use as a hydrogen separation material. Many of these effects however, can be completely mitigated through alloying palladium with another metal. By forming an alloy with a metal which has a lattice parameter similar to that of the β-phase the average difference between the sizes of the two phases is effectively decreased and thus the hydrogen embrittlement effect can be effectively mitigated. The effect of impurities on palladium membranes can also be partially mitigated by alloying with another metal and oftentimes an increase in permeability is reported with certain alloy compositions.

Both binary and ternary alloys of palladium have been reported and is a mature topic in literature. By far the three most popular alloying compounds with palladium are silver, copper and gold. The current literature landscape of palladium alloy membranes are summarised in Table 2.4 and for the purpose of this review studies which looked at the impurity resistance, which is currently the most pressing issue in the field, were focused on.

Silver is the most popular dopant for palladium membranes and forms a stable alloy with palladium at concentrations greater than 20wt %, with the optimal composition occurring at 23%. On top of mitigating the effects of hydrogen embrittlement, a 60% increase in permeability is observed when compared to pure Pd membranes. Despite having enhanced permeation properties, PdAg is still susceptible to poisoning, in particular from sulphurous compounds which can form both Pd_4S and $Ag_5Pd_{10}S_5$. Several studies exposing PdAg membranes to sulphurous compounds have been performed and in most cases the membranes suffer a large decrease in flux, and are permanently damaged as shown by a permanent decrease in flux when sulphide is removed from the inlet. [43] It has been observed that exposure to 5 µmol mol^{-1} H_2S in the feed stream is enough to induce Pd_4S formation [43] and therefore this composition is only suitable for atmospheres and applications which do not contain any sulphur.

Copper is another widely studied binary alloy which is known to suppress hydrogen embrittlement. Alloying with copper also has the advantage that it reduces the cost

of the membrane by a larger amount than most other metals and through improving the membranes sulphur resistance. The maximum permeability of a palladium copper membrane occurs at the composition $Pd_{60}Cu_{40}$ and this is due to the formation of a bcc lattice rather than the fcc lattice commonly seen in pure palladium and most binary alloys. [44] Temperature cycling has been performed on this alloy composition and it has been found that the bcc crystalline configuration has a higher permeability than the fcc phase. [45] This behaviour is due to the increased number of hcp adsorption sites which hydrogen has a slight preference for.[46] Conversely the fcc structure has a higher impurity resistance than the bcc structure, particularly for H_2S. This has been theorised to be because adsorption of H_2S on a palladium membranes surface is largely controlled by electronic factors.[47] There have been several studies reporting an increased resistance to sulphur poisoning by alloying palladium with copper. A $Pd_{80}Cu_{20}$ membrane exposed to 20 µmol mol^{-1} of H_2S for 90 hours results in a 22% drop in flux, performing much better than $Pd_{75}Ag_{25}$ reported in the same paper which became impermeable after 65 hours of exposure in the same conditions.[43] In a similar study, the performance of bcc and fcc alloys in response to H_2S $Pd_{20}Cu_{80}$, $Pd_{40}Cu_{60}$ and $Pd_{53}Cu_{47}$ foils at varying temperatures was tested in hydrogen containing 1000 µmol mol^{-1} H_2S.[48] It was found that when the alloys were in the fcc phase the reduction in flux was only round 10%, while in the bcc phase the membrane loses around 99% of its permeance. The H_2S concentration required to make a $Pd_{60}Cu_{40}$ membrane completely impermeable was found to be around 300 µmol mol^{-1} [49].

PdAu alloys see a slight increase in permeability, up to 30% more than pure Pd, with gold additions up to 20%, after which the permeability rapidly decreases. While alloying with gold does not improve the permeability much compared to silver or copper, gold alloys show greatly improved sulphur resistance. Several studies have been performed which show that PdAu membranes show no permanent permeability loss after exposed to ppm levels of sulphurous compounds implying that permeability decline is only due to H_2S adsorption. It has been reported that a $Pd_{92}Au_8$ membrane exposed to 54.8 µmol mol^{-1} of H_2S was able to resist reaction with H_2S and its permeability was completely recoverable. [50]. When tested higher temperatures it was also found that the adsorption effect of H_2S was reduced which is evidence that dissociative adsorption of H_2S on metals is exothermic. [50] In the original patent for palladium membranes by McKinley [51] in 1964 $Pd_{60}Au_{40}$ was found to be the composition which performed best under sulphur containing atmospheres, losing only 9.44% of its flux compared to the 99% and 95% lost by PdAg and PdCu membranes respectively.[51] However under recovery the flux increased to 120% of its original value while the PdCu membrane was fully recovered under the same conditions. This may be evidence that the $Pd_{60}Au_{40}$ membrane used is not completely stable. [51] When comparing the performance of PdCu and PdAu membranes under a number of gases which commonly result from the water gas shift reaction it was found that the PdAu resisted . [52] It was found that from the four membranes tested, the PdAu membranes show no permeability loss under an atmosphere containing CO, CO_2 and H_2O while the PdCu membranes showed considerable permeability loss. [52] The biggest downside to alloying with gold is that due to its high price in recent years alloying palladium with gold drives up the price higher than that

of a pure palladium membrane and is one of the less economic options. [53]

Other metals have been alloyed with palladium although outside of these three metals, studies evaluating the impurity resistance of other binary alloys are rare. The adsorption of CO on $Pd_{92}Y_8$ membranes under various concentrations has been studied using TDS and XPS and found that CO can react with the Pd-Y allow at 623K, forming YO and solid carbon. [54] Bryden et al studied the poisoning resistance of nanostructured palladium-iron alloys compared to polycrystalline membranes of the same composition. [55] They found that nanostructured membranes not only display higher fluxes, but also exhibit a higher resistance to hydrogen sulphide poisoning. When exposed to ˜60 µmol mol^{-1}, of H_2S for 2.2 hours there was no permanent reduction in flux. Howard et al studied the performance of $PdPt_{20}$ membranes under 1000 µmol mol^{-1} H_2S at temperatures between 350°C and 450 °C. [56] The alloy had decent performance on the lower end of the temperature, only losing about 5% of permanent permeability. At higher temperatures the membrane lost around 25% of its permeability, much of this attributed to platinum segregation to the surface of the membrane.[56] The impurity resistance of PdPt membranes has also been studied under common WGS compositions which concluded that small additions of Pt (Between 5-9%) can decrease the flux decline caused by WGS mixtures from 39% for pure Pd, to anywhere between 7%-22%.[56] Platinum however does not appear to be as effective at mitigating the effects of WGS mixtures as alloying with Au which can completely mitigate the flux decline. [57] The use of $Pd_{95}Ru_5$ membranes in syngas mixtures has been tested in WGS conditions and also showed good resistance to adsorbing compounds, losing only 6% of their flux compared to the 11% lost by a pure Pd membrane under the same conditions.[58]

Ternary alloys are a newly emerging field which aims at utilizing the strengths of a binary alloy while mitigating its weaknesses with another component. Research in this area has mainly focused on ternary alloys based on copper, gold and silver however there are theoretically infinite combinations possible. A $Pd_{80}Au_{10}Pt_{10}$ membrane manufactured through magnetron sputtering was found to be completely resistant to H_2S poisoning, recovering 100% of its flux prior to exposure to impurity containing gas streams. [59] However after long term testing, the purity of the permeate decreased which implies that pinholes had started to form on the membrane surface. [59] This is most likely due to segregation of the individual components, destabilising the structure. This was not confirmed in the papers analysis however. [59] The most in depth study of PdAgAu membranes under H_2S was performed by Braun et al, who studied the performance of Pd, $Pd_{90}Ag_{10}$, $Pd_{78}Ag_9Au_{13}$, $Pd_{75}Ag_{16}Au_9$, and $Pd_{91}Au_9$. While all the tested membranes saw a permanent permeability loss under 100 µmol mol^{-1} of H_2S the $Pd_{91}Au_9$, $Pd_{78}Ag_9Au_{13}$, and $Pd_{75}Ag_{16}Au_9$ all resisted bulk corrosion as proven by Energy-dispersive X-ray spectroscopy (EDS), with the $Pd_{91}Au_9$ sample having the highest resistance to H_2S atmospheres. [60, 61] While this study shows that ternary alloys do offer an increase in impurity resistance over pure Pd and PdAg membranes, the original flux values are not provided so it is difficult to see if there are any inherent advantages over simply using a PdAu alloy. [60, 61] The Materials and Chemistry group at SINTEF have performed the most extensive study into ternary alloys, [62, 63] testing by far the widest range of alloys and using a combination of X-ray Diffraction

(XRD) and X-ray photoelectron spectroscopy to analyse the segregation behaviour of the ternary alloys. [62, 63] Through alloying PdCu alloys with a third transition metal they found that the addition of 1% of a transition metal component always resulted in an increase in permeability, likely due to a phenomenon where the activation energy for hydrogen permeation decreases with increasing fcc lattice constant. [64] In particular the addition of 1% Ta, 1% Y and 14% Ag resulted in an increase in permeability of 10, 45 and 65% respectively when compared with $Pd_{73}Cu_{27}$ membranes for Y and Ta, and $Pd_{65}Cu_{35}$ membranes for Ag additions. [64] In the follow up paper $Pd_{75}Ag_{22}Au_3$, $Pd_{76}Ag_{21}Mo_3$ and $Pd_{69}Ag_{27}Y_4$ membranes were exposed to 20 µmol mol^{-1} of H_2S for 500 hours. The $Pd_{75}Ag_{22}Au_3$ membrane was the only membrane which showed no bulk sulphur formation, with the other two membrane compositions showing large levels of oxidation and segregation when analysed using XPS. [65] The PdAgAu composition has been further studied by Braun et al, [61] who backed up that small additions of Au to PdAg membranes can reduce the membranes reactivity with sulphides and would be suitable for application in a hydrogen impurity enrichment device. Tarditi et al, have done a similar study on the impurity resistance of PdCuAu membranes. [66] While XRD and EDS of this alloy showed no formation of bulk sulphides, the XPS depth profile showed low, but measurable levels of sulphur showing that this composition has some reactivity with impurities. [66]

Table 2.4: Review of palladium alloys and their interactions with impurities

Membrane composition	Support	Susceptability to poisoning compounds					Pressure (bar)	Permeability $molm^{-1}s^{-1}pa^{-\frac{1}{2}}$	Temperature °C	Fabrication technique	Membrane thickness (µm)	Ref
		Compound concentration	Exposure time	Percentage flux drop	Flux Recovery	Initial flux						
$PdAg_{23}$	PSS/Al_2O_3	19.2% CO_2, 15.4% H_2O, 4% CO, 1.2% CH_4	500h	88.36%	-	990 $cm^3cm^{-2}min^{-1}$	26	2.42×20^{-9}	400	Magnetron Sputtering	2.2	[67]
$PdAg_{23}$	PSS/Al_2O_3	40.5% CO_2, 25% H_2O, 2% CO, 2.5% CH_4	500h	94.65%	-	990 $cm^3cm^{-2}min^{-1}$	26	2.42×20^{-9}	400	Magnetron Sputtering	2.2	[67]
$PdAg_{23}$	PSS/Al_2O_3	60% CO_2, 25.5% H_2O, 2% CO, 2.5% CH_4	500h	94.65%	-	990 $cm^3cm^{-2}min^{-1}$	26	2.42×20^{-9}	400	Magnetron Sputtering	2.2	[67]
Pd	Self-supported	1000 ppm H_2S	6h	90%	-	14 $cm^3cm^{-2}min^{-1}$	3.1	1.2×20^{-8}	350	-	25	[48]
$PdCu_{53}$	Self-supported	1000 ppm H_2S	6h	90%	-	14 $cm^3cm^{-2}min^{-1}$	3.1	1.3×20^{-8}	350	-	25	[48]
Pd	PSS/Al_2O_3	54.8 ppm H_2S	24h	93%	0%	-	2.02	-	400	ELP	10.3	[50]
$PdAu_8$	PSS/Al_2O_3	54.8 ppm H_2S	24h	85%	54%	-	2.02	-	400	ELP/Electroplating	16	[50]
$PdAg_{23}$	PSS	2 ppm H_2S	10 minutes	7%	100%	66.7 $cm^3cm^{-2}min^{-1}$	-	1.9×10^{-8}	450	Magnetron Sputtering	10	[68]
$PdAg_{23}$	PSS	5 ppm H_2S	10 minutes	29%	100%	66.7 $cm^3cm^{-2}min^{-1}$	-	1.9×10^{-8}	450	Magnetron Sputtering	10	[68]
$PdAg_{23}$	PSS	2-5-2 ppm H_2S	10 minutes at 5ppm	25%	99.4%	51.5 $cm^3cm^{-2}min^{-1}$	-	1.9×10^{-8}	450	Magnetron Sputtering	10	[68]
$PdAg_{23}$	PSS	2-6.6-2 ppm H_2S	10 minutes at 6.6ppm	25%	36%	51.2 $cm^3cm^{-2}min^{-1}$	-	1.9×10^{-8}	450	Magnetron Sputtering	10	[68]
$PdAg_{23}$	PSS	2-10-2 ppm H_2S	10 minutes at 10ppm	83%	99.6%	51.2 $cm^3cm^{-2}min^{-1}$	-	1.9×10^{-8}	450	Magnetron Sputtering	10	[68]
$PdAg_{23}$	PSS	2-20-2 ppm H_2S	10 minutes at 20ppm	85%	100%	51.0 $cm^3cm^{-2}min^{-1}$	-	1.9×10^{-8}	450	Magnetron Sputtering	10	[68]
$PdAg_{23}$	PSS	5-20-5 ppm H_2S	10 minutes at 6.6ppm	71%	17.99%	18.9 $cm^3cm^{-2}min^{-1}$	-	1.9×10^{-8}	450	Magnetron Sputtering	10	[68]
Pd	PSS/Al_2O_3	111.8% CO_2, 5.3% H_2O, 14.2% CO, 1.7% CH_4 51% N_2	48h	11%	-	-	0.1	-	350	ELP	6.5	[69]

Pd	PSS/Al_2O_3	11.8% CO_2, 5.3% H_2O, 14.2% CO, 1.7% CH_4 51% N_2 120 mg/m^3 tar	24h	66.7%	-	-	0.1	-	350	ELP	6.5	[69]
Pd	PSS/Al_2O_3	111.8% CO_2, 5.3% H_2O, 14.2% CO, 1.7% CH_4 51% N_2 240 mg/m^3 tar	24h	100%	-	-	0.1	-	350	ELP	6.5	[69]
$PdRu_5$	PSS	11.8% CO_2, 5.3% H_2O, 14.2% CO, 1.7% CH_4 51% N_2	48h	6%	-	-	0.1	-	350	ELP	7.3	[69]
$PdRu_5$	PSS	11.8% CO_2, 5.3% H_2O, 14.2% CO, 1.7% CH_4 51% N_2 120 mg/m^3 tar	24h	66.7%	-	-	0.1	-	350	ELP	7.3	[69]
$PdRu_5$	PSS	11.8% CO_2, 5.3% H_2O, 14.2% CO, 1.7% CH_4 51% N_2 240 mg/m^3 tar	24h	93%	-	-	0.1	-	350	ELP	7.3	[69]
Pd	YSZ	50% NH_3	75h	0%	-	0.056.0 $molm^{-2}s^{-1}$	2-7	-	400	ELP	1.6	[70]
$PdAg_{25}$	PSS	0.5%CO	Until stable	80%	-	-	-	-	400	-	100	[71]
$PdAg_{25}$	PSS	0.5%CO	Until stable	4%	-	-	-	-	573	-	100	[71]
$PdAg_{25}$	PSS	0.5%CO	Until stable	0%	-	-	-	-	773	-	100	[71]
$PdAg_{25}$	PSS	1.5%CO	Until stable	91%	-	-	-	-	400	-	100	[71]
$PdAg_{25}$	PSS	1.5%CO	Until stable	7%	-	-	-	-	573	-	100	[71]
$PdAg_{25}$	PSS	1.5%CO	Until stable	0%	-	-	-	-	773	-	100	[71]
$PdAg_{25}$	PSS	10%CO	Until stable	98%	-	-	-	-	400	-	100	[71]
$PdAg_{25}$	PSS	10%CO	Until stable	50%	-	-	-	-	573	-	100	[71]
$PdAg_{25}$	PSS	10%CO	Until stable	0%	-	-	-	-	773	-	100	[71]
$PdAg_{25}$	PSS	20%CO	Until stable	99.8%	-	-	-	-	400	-	100	[71]
$PdAg_{25}$	PSS	20%CO	Until stable	50.5%	-	-	-	-	573	-	100	[71]
$PdAg_{25}$	PSS	20%CO	Until stable	0%	-	-	-	-	773	-	100	[71]
Pd	PSS	0.1%H_2S	120h	75%	-	$8.5cm^3cm^{-2}min^{-1}$	-	4×10^{-8}	350	-	100	[72]
Pd	PSS	0.1%H_2S	120h	82%	-	$13.5cm^3cm^{-2}min^{-1}$	-	4×10^{-8}	450	-	100	[72]

Pd	PSS	0.1% H_2S	120h	81%	-	$27.5 cm^3 cm^{-2} min^{-1}$	-	4×10^{-8}	550	-	100	[72]
Pd	PSS	12% CO, 12% N_2	Until stable	22%	-	$8.5 cm^3 cm^{-2} min^{-1}$	3	-	380	ELP	10	[73]
Pd	PSS	1.6% Steam, 1.6% N_2	Until stable	17%	-	$12.87 cm^3 cm^{-2} min^{-1}$	3	-	380	ELP	10	[73]
Pd	-	20 ppm H_2S, 40% N_2	115h	71.88%	-	-	31	1.5×10^{-8}	320	-	100	[43]
$PdAg_{25}$	-	10 ppm H_2S, 20% N_2	65h	100%	-	$27.5 cm^3 cm^{-2} min^{-1}$	31	1.4×10^{-8}	320	-	130	[43]
$PdCu_{20}$	-	20 ppm H_2S, 40% N_2	90h	22%	-	-	31	-	320	-	130	[43]
$PdCu_8$	PSS	42.7 ppm H_2S	2.5h	82%	86.67%	-	2	-	450	ELP	14	[74]
$PdAg_{27}$	-	4.4 ppm H_2S	48h	99%	67%	$3.7 cm^3 cm^{-2} min^{-1}$	5.17	-	350	-	920	[51]
$PdCu_{40}$	-	4.5 ppm H_2S	72h	95%	100%	$2.9 cm^3 cm^{-2} min^{-1}$	5.17	-	350	-	1030	[51]
$PdAu_{40}$	-	4.7 ppm H_2S	72h	9.4%	120%	$0.99 cm^3 cm^{-2} min^{-1}$	5.17	-	350	-	820	[51]
Pd	-	4.7 ppm H_2S	96h	70.1%	10%	$1.8 cm^3 cm^{-2} min^{-1}$	5.17	-	350	-	900	[51]
$PdAu_{40}$	-	20.6 ppm H_2S	168h	56.6%	120%	$0.99 cm^3 cm^{-2} min^{-1}$	5.17	-	350	-	790	[51]
$PdAu_{40}$	-	6.6% H_2S	6h	99%	120%	$0.99 cm^3 cm^{-2} min^{-1}$	5.17	-	350	-	810	[51]
$PdFe_6$	PSS	59.1 ppm H_2S	2.2h	75%	100%	$8.8 cm^3 cm^{-2} min^{-1}$	1	-	200	Electroplating	10	[55]
$PdFe_6$	PSS	59.1 ppm H_2S	2.2h	95%	100%	$6.4 cm^3 cm^{-2} min^{-1}$	1	-	200	Electroplating	10	[55]
$PdFe_5$	PSS	1% CO	4.2h	83.3%	-	$5.5\ cm^3 cm^{-2} min^{-1}$	1	-	200	Electroplating	18	[55]
$PdFe_5$	PSS	1% CO	4.2h	79%	-	$3.9\ cm^3 cm^{-2} min^{-1}$	1	-	200	Electroplating	18	[55]
$PdCu_4$	Accusep	20% CO_2, 8% CO	2h	17%	-	$5.85\ cm^3 cm^{-2} min^{-1}$	1.38	-	350	-	7	[52]
$PdAu_{13}$	Accusep	26% CO_2, 21% H_2O, 2% CO 50 ppm H_2S	13h	0%	-	$35.56\ cm^3 cm^{-2} min^{-1}$	4.96	-	350	-	7	[52]
$PdCu_4$	Accusep	26% CO_2, 21% H_2O, 2% CO 50 ppm H_2S	2h	70%	100%	$5.85\ cm^3 cm^{-2} min^{-1}$	4.96	-	350	-	7	[52]
$PdAu_{13}$	Accusep	26% CO_2, 21% H_2O, 2% CO 50 ppm H_2S	2h	0%	-	$35.56\ cm^3 cm^{-2} min^{-1}$	4.96	-	350	-	7	[52]
$PdAu_{10}$	Self-supported	30% CO_2, 19% H_2O, 1% CO	43h	32%	-	$0.28\ mol m^{-2} s^{-1}$	12.7	-	400	Magnetron Sputtering	-	[59]
$PdAu_{10}$	Self-supported	30% CO_2, 19% H_2O, 1% CO 20ppm H_2S	100h	70%	-	$0.28\ mol m^{-2} s^{-1}$	12.7	-	400	Magnetron Sputtering	-	[59]

$PdAu_{20}Pt_{10}$	Self-supported	30% CO_2, 19% H_2O, 1% CO	43h	30%	-	0.212 $molm^{-2}s^{-1}$	12.7	-	400	Magnetron Sputtering	-	[59]
$PdAu_{20}Pt_{10}$	Self-supported	30% CO_2, 19% H_2O, 1% CO	100h	100%	-	0.28 $molm^{-2}s^{-1}$	12.7	-	400		33	[59]
$PdAu_{10.2}$	PSS	20ppm H_2S 30% CO_2, 19% H_2O, 1% CO	350h	36%	-	0.21 $molm^{-2}s^{-1}$	6.27	-	400	Cold working	25	[57]
$PdAu_{10.2}$	PSS	30% CO_2, 19% H_2O, 1% CO	350h	72%	-	0.21 $molm^{-2}s^{-1}$	6.27	-	400	Cold working	25	[57]
$PdAu_{19}$	PSS	20 ppm H_2S 30% CO_2, 19% H_2O, 1% CO	350h	0%	-	0.25 $molm^{-2}s^{-1}$	6.27	-	400	Cold working	25	[57]
$PdAu_{19}$	PSS	30% CO_2, 19% H_2O, 1% CO	350h	0%	-	0.25 $molm^{-2}s^{-1}$	6.27	-	400	Cold working	25	[57]
$PdAu_7$	PSS	20 ppm H_2S 30% CO_2, 19% H_2O, 1% CO	350h	32%	-	0.47 $molm^{-2}s^{-1}$	6.27	-	400	Cold working	11	[57]
$PdAu_7$	PSS	30% CO_2, 19% H_2O, 1% CO	350h	68%	-	0.47 $molm^{-2}s^{-1}$	6.27	-	400	Cold working	11	[57]
$PdAu_{10.1}$	PSS	20 ppm H_2S 30% CO_2, 19% H_2O, 1% CO	350h	24%	-	0.36 $molm^{-2}s^{-1}$	6.27	-	400	Cold working	31	[57]
$PdAu_{10.1}$	PSS	30% CO_2, 19% H_2O, 1% CO	350h	62%	-	0.36 $molm^{-2}s^{-1}$	6.27	-	400	Cold working	31	[57]
Pd	ZrO_3/PSS	20 ppm H_2S 100 ppm H_2S	24h	85%	16%	-	-	1.21×10^{-8}	400	ELP	-	[61]
$PdAg_{10}$	ZrO_3/PSS	100 ppm H_2S	24h	75.7%	33%	-	-	1.65×10^{-8}	400	ELP	-	[61]
$PdAg_{16}Au_9$	ZrO_3/PSS	100 ppm H_2S	24h	73%	64.5%	-	-	1.18×10^{-8}	400	ELP	-	[61]
$PdAg_9Au_{13}$	ZrO_3/PSS	100 ppm H_2S	24h	66.67%	81%	-	-	1.34×10^{-8}	400	ELP	-	[61]
$PdAu_9$	ZrO_3/PSS	100 ppm H_2S	24h	60%	80%	-	-	0.99×10^{-8}	400	ELP	-	[61]
$PdAg_{23}$	Micro channel stainless steel	10% N_2, 20 ppm H_2S	1h	97.5%	67.5%	170 $cm^3cm^{-2}min^{-1}$	-	1.3×10^{-8}	450	Magnetron Sputtering	2.2	[63]
$PdAg_{22}Au_3$	Micro channel stainless steel	10% N_2, 20 ppm H_2S	1h	87.5%	80%	145 $cm^3cm^{-2}min^{-1}$	-	9.3×10^{-9}	450	Magnetron Sputtering	1.9	[63]

$PdAg_{27}Y_4$	Micro channel stainless steel	10% N_2, 20 ppm H_2S	1h	92.5%	65%	140 $cm^3cm^{-2}min^{-1}$	-	1.3×10^{-8}	450	Magnetron Sputtering	2.4	[63]
$PdAg_{21}Mo_3$	Micro channel stainless steel	10% N_2, 20 ppm H_2S	1h	97.5%	98%	75 $cm^3cm^{-2}min^{-1}$	-	5.8×10^{-8}	450	Magnetron Sputtering	2.3	[63]
$PdAg_{11}Mo_4$	Micro channel stainless steel	10% N_2, 20 ppm H_2S	1h	97.5%	96%	125 $cm^3cm^{-2}min^{-1}$	-	8.8×10^{-8}	450	Magnetron Sputtering	2.2	[63]
$PdAg_2Au_{15}$	Al_2O_3/PSS	1000 ppm H_2S	30h	-	-	-	-	1.3×10^{-8}	350	ELP	-	[60]
$PdAg_{14}Au_{12}$	Al_2O_3/PSS	1000 ppm H_2S	30h	-	-	-	-	-	350	ELP	-	[60]
Pd	PSS	1000 ppm H_2S	30h	-	-	-	-	1.2×10^{-8}	350	ELP	25	[60]
$PdCu_{65}$	ZrO_2/PSS	Varying	Varying	-	-	-	-	-	450	ELP	10	[49]
$PdCu_{73}$	ZrO_2/PSS	Varying	Varying	-	-	-	-	-	450	ELP	8	[49]
Pd	ZrO_2/PSS	Varying	Varying	-	-	-	-	-	450	ELP	4	[49]
Pd	ZrO_2/PSS	Varying	Varying	-	-	-	-	-	450	ELP	3	[49]
$PdCu_{32}$	ZrO_2/PSS	Varying	Varying	-	-	-	-	-	450	ELP	2	[49]
$PdCu_{20}$	ZrO_2/PSS	Varying	Varying	-	-	-	-	-	450	ELP	3	[49]
$PdCu_{40}$	ZrO_2/PSS	Varying	Varying	-	-	-	-	-	450	ELP	15	[49]
$PdCu_{40}$	ZrO_2/PSS	Varying	Varying	-	-	-	-	-	450	Cast rolled	25	[49]
$PdPt_{20}$	Self-supported	1000 ppm H_2S	150h	50%	95%	1.85 $mLcm^{-2}min^{-1}$	6.2	-	350	Mettalurgical	100	[56]
$PdPt_{20}$	Self-supported	1000 ppm H_2S	125h	80%	75%	2.95 $mLcm^{-2}min^{-1}$	6.2	-	400	Mettalurgical	100	[56]
$PdPt_{20}$	Self-supported	1000 ppm H_2S	125h	25%	75%	3.55 $mLcm^{-2}min^{-1}$	6.2	-	450	Mettalurgical	100	[56]
PdY_8	-	2-26% CO	-	-	-	-	0.06	-	Varying	-	-	[54]
Pd	-	SO_2 CS_2 H_2S	-	-	-	-	0.07 mBar	-	Varying	-	-	[75]
$PdCu_{20}$	Inconel	1000 ppm H_2S	-	-	-	-	-	-	Varying	Vacuum arc welding	100	[76]
$PdCu_{40}$	Inconel	1000 ppm H_2S	-	-	-	-	-	-	Varying	Vacuum arc welding	100	[76]
$PdCu_{47}$	Inconel	1000 ppm H_2S	-	-	-	-	-	-	Varying	Vacuum arc welding	100	[76]
Pd	PSS	100 ppm H_2S	24h	36%	80%	0.0475 $molm^{-2}s^{-1}$	0.5	1.2×10^{-8}	400	ELP	4	[77]
$PdAu_9$	PSS	100 ppm H_2S	24h	59%	75%	0.05 $molm^{-2}s^{-1}$	0.5	9.9×10^{-9}	400	ELP	4	[77]
$PdCu_{25}Au_5$	PSS	100 ppm H_2S	24h	50%	74%	0.01 $molm^{-2}s^{-1}$	0.5	1.9×10^{-9}	400	ELP	4	[77]
$PdCu_{37}Au_3$	PSS	100 ppm H_2S	24h	54%	70%	0.015 $molm^{-2}s^{-1}$	0.5	2.9×10^{-9}	400	ELP	4	[77]
$PdAu_{23}$	Accusep	20 ppm H_2S	96h	29%	97%	1.4 $molm^{-2}s^{-1}$	11	1.55×10^{-8}	500	ELP	4.8	[78]
$PdAu_{20}Ag_{13}$	Accusep	20 ppm H_2S	96h	50%	89%	0.9 $molm^{-2}s^{-1}$	11	1.65×10^{-8}	500	ELP	9.3	[78]

Non-palladium

Due to the high cost of palladium there is a particular interest to use alternative materials which still give the high selectivity intrinsic to dense metallic membranes, while reducing the cost, for example, by switching to a cheaper, non-platinum group metal. Non-palladium alloy membranes in the form of amorphous, or crystalline structures generally attract the most research interest.

Crystalline non-palladium membranes are generally based on Group IV based alloys and follow a similar philosophy to the previously discussed palladium membranes. Group IV metals are alloyed with other metals in order to improve their physical properties while maintaining the bcc structure essential for the material to transport hydrogen. Crystalline metals typically have the same advantages and disadvantages as palladium membranes. Recent research activity has focused mainly on studying how the size of the grain boundary affects the permeability of such a membrane, an area which has been mostly neglected in palladium research. [31] This is likely due to the fact that many of these alloys are manufactured through cold work where the grain size can be more easily tailored than in the traditional electroless and sputtering methods used to manufacture palladium membranes. A key aspect of crystalline alloy research is the effect of nano-crystalline structures. Most research in this area has revolved around the addition of small amounts of elements to alloys based on either Zr or Hf to tailor these nano-crystalline structures and study their effects on permeability. Similarly to palladium alloys, dopants are generally chosen based on their effectiveness at suppressing hydride formation, with Zr, Mo, Ru and Rh being popular choices. [79, 80, 81, 82, 83] Alloying in this context would also likely be useful in reducing the membranes interaction with impurities through surface contamination. However this has not been touched upon much in research outside of palladium. The largest drawback to this technology is that crystalline alloys often do not show the catalytic activity necessary for dissociation of hydrogen. This requires an additional coating of palladium to be applied to the surface in order for the material to be viable for hydrogen separation. Interestingly when this was done with some commonly used industrial alloys [84] it was found that they showed reasonable hydrogen permeability which further highlights the importance of catalytic dissociation of hydrogen. Crystalline membranes are also mechanically weak and still susceptible to hydrogen embrittlement through hydride formation in a similar manner to palladium membranes. [31]

On the other hand amorphous metal membranes are generally seen as more attractive than crystalline membranes and are often reported to have greater mechanical strength and hydrogen solubility properties than crystalline structures due to their amorphous structure giving them a more open lattice. Unlike crystalline structures, amorphous metallic membranes can also have high catalytic activity towards hydrogen dissociation which reduces the need for an additional layer to induce this catalytic activity. This property is highly composition dependent and is typically shown by Nickel containing alloys. [85] For example $Zr_{36}Ni_{64}$ in its pure form due to the presence of nickel which is catalytically active for hydrogen dissociation, however when researchers started to dope the material with Ti or Hf, the catalytic properties of the material was drastically

reduced and required a layer of palladium in order to induce permeability.

Amorphous membranes still show some tendency towards hydrogen embrittlement however this is less prevalent than the crystalline alloys previously discussed. This is due to the differences in mechanisms of hydrogen embrittlement between the two classes of materials. Amorphous alloys do not show the α-β phase transition which is the main suspect of embrittlement in crystalline structures [85] and the embrittlement effect is instead due to the filling of free volume within the amorphous structure.

The main disadvantage of amorphous alloys is that given sufficient energy amorphous metallic membranes may crystallise, drastically changing their structure. This has been reported when the material is heated to high temperatures above 500°C. [85] This limits the application of amorphous alloys to low-temperatures however if the material is intended to be used at 300°C, like most palladium membranes, and the material shows a high enough permeability, then this would likely not be an issue.

Judging from the current research landscape on non-palladium membranes, the technology is still in its infancy, with most studies focusing on the fundamental properties of these alloys and with little focus on the practical applications of the technology. Non-palladium dense metal membranes are promising due to the drastic reduction in material cost with, in many cases, an increase in permeability. Of these technologies amorphous membranes appear to be the most appealing, in particular compositions such as $Zr_{36}Ni_{64}$ which require no precious metals to induce catalytic activity. This has the great advantage of reducing cost of the module and bringing dense metallic membranes, and their high associated selectivity, to a wider market by taking advantage of already established industrial production of amorphous alloys. Further practical research must be performed on these membrane compositions, in particular impurity interactions, thermal stability, and long-term stability to bring this technology to market.

Table 2.5: Hydrogen permeable non-palladium metallic membranes

Membrane composition	Structure	Catalytic coating	Feed pressure	Permeability mol m^2 m s	Temperature °C	Membrane thickness (µm)	Ref
$(Ni_{0.6}Nb_{0.4})_{70}Zr_{30}$	Amorphous	Pd	7	1.8×10^{-8}	400	40	[86]
$(Ni_{0.6}Nb_{0.4})_{60}Zr_{40}$	Amorphous	Pd	7	6×10^{-9}	400	40	[86]
$Ni_{65}Nb_{25}Zr_{10}$	Amorphous	Pd	7	5×10^{-9}	400	40	[86]
$Ni_{45}Nb_{45}Zr_{10}$	Amorphous	Pd	7	3×10^{-9}	400	40	[86]
$Ni_{60}Nb_{40}$	Amorphous	Pd	7	2×10^{-9}	400	40	[86]
$Ni_{44}Nb_{43}Zr_{10}Pd_3$	Amorphous	Pd	7	1×10^{-9}	400	40	[86]
$Zr_{36}Ni_{64}$	Amorphous	None	1	1.2×10^{-9}	350	30	[87]
$(Ni_{0.6}Nb_{0.4})_{45}Zr_{50}Al_5$	Amorphous	Pd	3	1.9×10^{-8}	400	50	[88]
$(Ni_{0.6}Nb_{0.4})_{45}Zr_{50}Co_5$	Amorphous	Pd	3	2.46×10^{-8}	400	50	[88]
$(Ni_{0.6}Nb_{0.4})_{45}Zr_{50}Cu_5$	Amorphous	Pd	3	2.34×10^{-8}	400	50	[88]
$(Ni_{0.6}Nb_{0.4})_{45}Zr_{50}Pd_5$	Amorphous	Pd	3	1.36×10^{-8}	400	50	[88]
$V_{85}Ni_{15}$	Crystalline	Pd	0.8	5×10^{-8}	300	300-400	[89]
$V_{95}Ni_{15}$	Crystalline	Pd	0.1-2.0	4×10^{-7}	400	2000	[90]
$V_{85}Ni_{14.91}Al_{0.09}$	Crystalline	Pd	0.1-2.0	4.5×10^{-7}	400	2000	[90]
$V_{85}Ni_{14.1}Al_{0.9}$	Crystalline	Pd	0.1-2.0	4.5×10^{-7}	400	2000	[90]
$V_{85}Ni_{12.4}Al_{2.6}$	Crystalline	Pd	0.1-2.0	6×10^{-7}	400	2000	[90]
$V_{85}Ni_{10.5}Al_{4.5}$	Crystalline	Pd	0.1-2.0	7×10^{-7}	400	2000	[90]
$V_{90}Al_{10}$	Crystalline	Pd	0.2 – 2.0	2×10^{-7}	900	800-2300	[91]
$V_{70}Al_{30}$	Crystalline	Pd	0.2 – 2.0	1.8×10^{-9}	700	800-2300	[91]
INCOLOY903	Crystalline	Pd	1	1.33×10^{-7}	430	200	[84]

WASPALOY	Crystalline	Pd	1	2.99 $\times 10^{-7}$	430	200	[84]
JBK-75	Crystalline	Pd	1	4.36 $\times 10^{-7}$	430	200	[84]
GH85A	Crystalline	Pd	1	2.73 $\times 10^{-7}$	430	200	[84]
INCOLOY907	Crystalline	Pd	1	9.67 $\times 10^{-8}$	430	200	[84]
INCONEL718	Crystalline	Pd	1	2.22 $\times 10^{-7}$	430	200	[84]
GH761	Crystalline	Pd	1	1.5 $\times 10^{-7}$	430	200	[84]
$Nb_{20}Zr_{35}Ni_{35}$	Crystalline	Pd	1	2.73 $\times 10^{-8}$	400	500-700	[92]
$Nb_{10}Zr_{45}Ni_{45}$	Crystalline	Pd	1	2.5 $\times 10^{-8}$	400	500-700	[92]
$Nb_{29}Ti_{31}Ni_{40}$	Crystalline	Pd	2	7 $\times 10^{-9}$	400	550-750	[93]
Nb17Ti42Ni41	Crystalline	Pd	2	0.6 $\times 10^{-8}$	400	550-750	[93]
Nb10Ti50Ni40	Crystalline	Pd	2	4.5 $\times 10^{-9}$	400	550-750	[93]
Nb39Ti31Ni30	Crystalline	Pd	2	2.0 $\times 10^{-8}$	400	550-750	[93]
Nb28Ti42Ni30	Crystalline	Pd	2	1 $\times 10^{-8}$	400	550-750	[93]
Nb21Ti50Ni29	Crystalline	Pd	2	1 $\times 10^{-8}$	400	550-750	[93]
$Ta_{95}W_5$	Crystalline	None	1.4	52 $molm^{-2}s^{-1}$	500	650	[94]

Dense Ceramic

Dense ceramic membranes operate in a similar manner to metallic membranes, with the key difference being that they are made from ion conducting ceramics rather than metals. Dense ceramic membranes have a selectivity comparable to dense metal membranes since they only allow hydrogen to permeate, however at a lower cost than Pd-based membranes. Unlike dense metallic membranes, most ion conducting materials claim to be intrinsically inert to common hydrogen impurities and hence are stable in CO, CO_2 and H_2S containing atmospheres. [31] The major drawback to ion conducting ceramic membranes is that generally high temperatures are required to achieve any form of H_2 flux. While palladium membranes can achieve a high flux at temperatures between 300-400°C, most Perovskite membranes require temperatures between 700-900°C and generally only achieve a hydrogen permeability <10% compared to a palladium membrane of the same thickness.

The hydrogen separation process in a dense ceramic membrane is near identical to that which occurs in a dense metal membrane with the main driving forces being the pressure and concentration gradients. This is primarily controlled by the catalytic surface effects and bulk diffusion rather than thickness due to ceramic materials intrinsically low catalytic activity for such a process. For practical purposes both sides of the membrane should have sufficient catalytic activity to dissociate hydrogen atoms and the bulk should have high enough proton and electron conductivities to ensure a reasonably high flux can be achieved. More information on the precise mechanism behind proton conducting membranes can be found in the following reviews [95, 96]. The bulk diffusion of a dense ceramic membrane can be described through the Wagner equation written as Eq 2.21

$$J_{H_2} = \frac{RT}{4F^2L}\frac{\theta_H\theta_e}{\theta_H+\theta_e}ln\left(\frac{P'_{H_2}}{P''_{H_2}}\right) \tag{2.21}$$

Dense ceramic membranes can be split into two broad categories; single phase ceramic membranes are composed of a single material which has the ability to conduct both protons and electrons, and multi-phase ceramic membranes which are normally composed of two or more phases which when combined show proton and electron conductivity. The most common type of multi-phase ceramic membranes is known as 'cermet' which combines a proton conducting ceramic and a metal, such as palladium or nickel, as the electron conducting phase.

Single phase ceramic membranes must be given proton conductivity by doping a single phase ceramic material (typically perovskite) in order to create a proton hole within the material. This combined with catalytic dissociation of hydrogen on the surface allows uptake of a certain number of protons, which then diffuse through the material using the proton holes within the material. [95, 96]

Extensive efforts have been placed into developing proton-electron conducting ceramic materials for hydrogen separation however there are still many technical hurdles which must be overcome before the technology can be applied on a useful scale. The

main problem holding back the technology is the incredibly low flux values reported despite operating at such high temperatures. Until this is solved there will be no point in using the technology over faster porous materials, or even dense metal membranes which offer the same selectivity's, at much faster permeation rates. This stems back to a lack of understanding behind the surface kinetics of hydrogen dissociation (which is also an issue for non-palladium dense membranes). Despite claims that ceramic membranes are inert to impurities there is contradictory evidence showing that the materials cannot withstand acidic conditions and degrade under atmospheres containing CO_2 and H^2S. Finally, since such high temperatures are required there will be difficulties forming a hermetic seal with ceramic membranes which can withstand the high temperature environments. This is already an issue with ceramic supported metallic membranes which operate at much more mild conditions.

From this it can be concluded that dense ceramic membranes for hydrogen separation are still at a research level and a better understanding of the material science behind the surface interactions with hydrogen and other gases, along with research into new classes of ceramics which can either permeate hydrogen at faster rates, at lower temperatures, or both are key to bringing this technology to market.

Table 2.6: Hydrogen permeable ceramic and cermet membranes which show resistance to common hydrogen impurities

Material	Class	Feed	Temperature °C	Flux	Thickness (µm)	Stability	Notes	Ref
$SrCe_{0.75}Zr_{0.2}Tm_{0.05}O_{3-\alpha}$	Perovskite	100 $mLmin^{-1}$ 50% H_2 + He	900	0.042 $mLcm^{-2}min^{-1}$	1200	-	-	[97]
$Nd_{5.5}WO_{12-\alpha}$	Lanthanide tungstate	80% He + 20 % H_2	1000	0	900	Stable under 115 ppm H_2S, 4.43% CO_2, 2.12% CO	No flux due to dry conditions	[98]
$La_{5.5}WO_{11.25}$	Lanthanide tungstate	80% He + 20 % H_2	1000	$< 0.005 mLmin^{-1}cm^{-2}$	900	Stable in 15% CO_2 for 3 days	Requires humidification for faster permeation	[99]
Nd_6Wo_{12}	Lanthanide tungstate	He + H_2	1000	0.012 $mLmin^{-1}cm^{-2}$	510	Stable in CO_2 and CH4 after 3 days	Humidified atmosphere	[100]
$La_{5.5}W_{0.8}Re_{0.2}O_{11.25-\alpha}$	Lanthanide tungstate	2.5% H_2, 2.5% H_2O, H_2 balance	1000	$0.095 mLmin^{-1}cm^{-2}$	760	Stable in 5% CO_2 1000 ppm COS 100 ppm HCN 46% CO 46% H_2 at 35 bar	Humidified atmosphere	[101]
$(La_{5/6}Nd_{1/6})_{5.5}WO_{12-\alpha}$	Lanthanide tungstate	80% He + 20 %H_2	1000	$0.005 mLmin^{-1}cm^{-2}$	900	Stable in 15% CO_2 for 3 days	Requires humidification	[102]
$La_{27}Mo_{1.5}W_{3.5}O_{55.5}$	Lanthanide tungstate	10% H_2 90% He	700	$0.78 \times 10^4 mLmin^{-1}cm^{-2}$	650	-	-	[103]
$La_{27}Mo_{1.5}W_{3.5}O_{55.5}$	Lanthanide tungstate	10% H_2 90% He	700	$0.78 \times 10^4 mLmin^{-1}cm^{-2}$	650	-	-	[103]
$Nd_{5.5}W_{0.5}Mo_{0.5}O_{11.25-\alpha}$	Lanthanide tungstate	50% H_2, 50% He	1000	0.235 $mLcm^{-2}min^{-1}$	900	Stable in environments containing 330 ppm H_2S and 22% H_2 in N_2. 480 ppm H_2S and 32% H_2 in N_2. 705 ppm H_2S and 47% H_2 in N_2 1500 ppm H_2S and H_2.	Values for humidified atmosphere. Stabilised flux value after 3 sets of tests Flux reduction due to Mo reduction	[104]
$Ni - Ba(Zr_{0.7}Pr_{0.1}Y0.2)O_{3-\alpha}$	Cermet	40% H_2, 57% N2, 3% H_2O	900	$1.36 \times 10^8 molcm^{-2}s^{-1}$	400	Stable under 30% CO_2	Maximum value achieved for humid atmosphere	[105]
$Ni - Ba(Zr_{0.1}Ce_{0.7}Y_{0.2})O_{3-\alpha}$	Cermet	20% H_2, 77% N2, 3% H_2O	900	$1.37 \times 10^{-7} molcm^{-2}s^{-1}$	30	-	Maximum value achieved for humid atmosphere	[106]
$La_{27}W_5O_{55.5} - LaCrO_3$	Dual phase ceramic	50% H_2 (humid)	700	$0.384 \times 10^{-3} mLcm^{-2}min^{-1}$	1210	-	Pt coating	[107]
$La_{5.5}WO_{11.25-\alpha} - La_{0.87}Sr_{0.13}CrO_{3-\alpha}$	Dual phase ceramic	50% H_2, 2.5%H_2O	700	$0.15 mLcm^{-2}min^{-1}$	360	Stable in 15% CO_2 after 24 hours.	No dry atmosphere testing	[108]
$Ni - La_{0.5}Ce_{0.5}O_{2-\alpha}$	Cermet	20% H_2, 80% N2	900	$5.64 \times 10^{-8} molcm^{-2}s^{-1}$	48	Stable in CO_2	Flux increased in humidified conditions	[109]
$Ni - Ca_{0.0125}La_{0.4875}Ce_{0.5}O_{2-\alpha}$	Cermet	20% H_2, 77% N2, 3%H_2O	900	$1.88 \times 10^{-8} molcm^{-2}s^{-1}$	600	Stable in CO_2	No dry atmosphere testing	[110]
$Ni - La_{0.5}Ce_{0.5}O_{2-\alpha}$	Cermet	20% H_2, 80% N2	900	$1.57 \times 10^{-8} molcm^{-2}s^{-1}$	600	Stable in CO_2	No dry atmosphere testing	[110]

$Ni - La_{0.5}Ce_{0.5}O_{2-\alpha}$	Cermet	20% H_2, 80% N2	900	$2.87 \times 10^{-8} molcm^{-2}s^{-1}$	600	-	No dry atmosphere testing	[111]
$BaZr_{0.8}Y_{0.15}Mn_{0.05}O_{3-\alpha}$	Perovskite	50% H_2, 50% He	1000	$0.01 - 0.03 mLcm^{-2}min^{-1}$	900	-	No dry atmosphere, Pt coated	[102]
$SrCe_{0.75}Zr_{0.2}Tm_{0.05}O_{3-\alpha}$	Perovskite	10% H_2, 90% He	900	$0.025 mL(STP)cm^{-2}min^{-1}$	1600	Stable in 20% CO_2 and 11.3% CO	-	[112]
$SrCe_{0.75}Zr_{0.2}Eu_{0.1}O_{3-\alpha}$	Perovskite	100% H_2	900	$0.35 cm^3cm^{-2}min^{-1}$	17	-	Flux improves in humid atmospheres	[113]
$Ni - BaCe_{0.7}Zr_{0.1}Y_{0.1}Yb_{0.1}O_{3-\alpha}$	Cermet	100% H_2	700	$0.49 mLcm^{-2}min^{-1}$	44	-	-	[114]
$Ni - BaCe_{0.7}Zr_{0.1}Y_{0.1}Yb_{0.1}O_{3-\alpha}$	Cermet	100% H_2	900	$1.12 mLcm^{-2}min^{-1}$	44	-	-	234
$BaCe_{0.95}Tb_{0.05}O_{3-\alpha}$	Perovskite	50% H_2 50% He	1000	$0.422 molcm^{-2}s^{-1}$	-	-	Hollow fibre	[114]
$BaCe_{0.85}Tb_{0.05}Co_{0.1}O_{3-\alpha}$	Perovskite	50% H_2 50% He	1000	$0.385 mLcm^{-2}min^{-1}$	167	Unstable in H_2	Hollow fibre. Also shows oxygen permeability	[115]
$Ni - BaCe_{0.7}Y_{0.1}Yb_{0.1}Zr_{0.1}O_{3-\alpha}$	Cermet	20% H_2, 20% CO_2, 60% N2	1000	$5.5 \times 10^{-8} molcm^{-2}s^{-1}$	44	Unstable in H_2	Shows reverse WGS catalytic activity, Stable in 60% CO_2. CO causes Ni corrosion	[116, 117]
$BaCe_{0.8}Y_{0.2}O_{3-\alpha}$	Perovskite	25% H_2 75% He	1050	$0.38 mLcm^{-2}min^{-1}$	1000	Unstable in humid environments and CO_2	Hollow Fibre	[118]
$La_{28-x}W_{4+x}O_{54+3x/2} (La = W \times 5.6)$	Lanthanum tungstate	10% H_2 90% Ar	925	$0.08 NmLcm^{-2}min^{-1}$	30	-	-	[119]
$La_{0.87}Sr_{0.13}CrO_{3-\alpha}$	Lanthanum tungstate	10% H_2, 2.5% H_2O 87.5% Ar	1000	$10 \times 10^{-4} mLcm^{-2}min^{-1}$	550	Chemically stable under tested conditions	-	[120]
$BaCe_{0.85}Tb_{0.05}Co_{0.1}O_{3-\alpha}$	Perovskite	50% H_2, 50% He	700-1000	$0.009 - 0.164 mL(STP)cm^{-2}min^{-1}$	132	-	Hollow fibre	[121]
$BaCe_{0.85}Tb_{0.05}Co_{0.1}O_{3-\alpha}$	Perovskite	50% H_2, 50% He	700-1000	$0.018 - 0.269 mL(STP)cm^{-2}min^{-1}$	132	-	Hollow fibre, Ni Coating	[121]
$BaCe_{0.85}Tb_{0.05}Co_{0.1}O_{3-\alpha}$	Perovskite	50% H_2, 50% He	700-1000	$0.1 - 0.42 mL(STP)cm^{-2}min^{-1}$	132	-	Hollow fibre, Pd Coating	[121]
$BaCe_{0.95}Tb_{0.05}O_{3-\alpha}$	Perovskite	50% H_2, 50% He	900	$0.272 mLcm^{-2}min^{-1}$	100	-	Hollow fibre, Pd Coating	[122]

Viable membrane materials and outlook

While ceramic membranes provide a viable alternative to metallic membranes as an impurity enrichment material, the technology is still in its infancy and the membranes do not show suitable permeabilities to perform impurity enrichment in a reasonable time frame. While many studies on these materials also claim that impurity resistance of these materials outclasses metallic membranes, there is little backing up these claims.

Of the membranes discussed, metallic membranes are the most suitable for hydrogen impurity enrichment. Palladium membranes are the only current material that has successfully been used for hydrogen impurity enrichment however there is still room for improvement which will be discussed in the following section. Non-palladium dense metallic membranes for hydrogen impurity enrichment are the next logical step in development of these membranes for analytical purposes due to their lower costs however more practical research on the materials must first be performed.

2.5.2 Membrane manufacture

Dense metal membranes can either be supported or unsupported. Unsupported membranes are free standing structures, which usually feature high wall thicknesses in order to achieve the required mechanical strength to withstand use in a process. As a result of this the flux seen through these membranes is typically low due to the high transport resistance of the membrane. Self-supported membranes are also typically expensive due to the large amount of materials required. [31]

A more efficient method is to use a support structure to allow a thinner membrane layer to be deposited, while achieving the mechanical strength required by use of another, cheaper material. This allows thinner membranes to be deposited, thereby increasing the achievable flux, and greatly reducing the cost of such a membrane.[31] Because of these clear advantages this thesis will explore the use of self-supported membranes.

Support selection

When selecting a support material there are a number of considerations which should be taken into account prior to deposition:

- Pore size distribution: If the supporting materials pore size distribution is too small then it will provide an added transfer resistance to permeation. The minimum thickness of a membrane deposited on a porous support has been found to be 3x the size of the smallest pore, [123] meaning there is a trade off betwen these two values
- Support surface: Adhesion of the deposited membrane to the surface of the support is compromised if the support is too smooth
- Thermal stability: The thermal stability of a support material is defined by the melting temperature, coefficient of thermal expansion (CTE) and intermetallic diffusion potential. If the CTE difference between the deposited membrane and

the support is too large it will lead to a difference in the expansion rate which eventually leads to membrane failure. Intermetallic diffusion is defined as the migration of atoms between the membrane and the substrate which can negatively affect it's permeability and lead to membrane failure in extreme cases

- Mechanical Stability
- Chemical stability

Of the materials available for use as a support; ceramics, porous stainless steel, and porous glass have been the most widely studied.

Glass

Porous glass supports are generally amorphous solids which feature pores ranging in sizes between the nanometre to micrometre range. They are commonly created through sol-gel synthesis, through metastable phase separation of borosilicate glasses, or by sintering glass powder. Porous glass supports have high thermal stability, and a narrow pore size distribution typically between 4-5 nm [124] [125], theoretically allowing membrane thicknesses of 8-10 nm to be achieved. [123] Despite this they arte extremely brittle and highly susceptible to acidic, alkaline or in the presence of metallic solutions. This limits their use in a number of common membrane manufacturing methods.

They are however extremely brittle and are highly susceptible to degradation under acidic, alkaline, or under metallic solutions which limits their use in a number of common membrane synthesis methods. [126]

Porous Stainless Steel (PSS)

Porous stainless steel is widely available in a large number of geometries and mainly see commercial use in a number of filtering applications. A membrane layer can be deposited on top of PSS in order to gain such properties as the high mechanical strength of PSS. PSS also features a similar CTE to palladium which limits the likelihood of membrane failure due to difference in expansion rate. They are however an expensive option, with 70% of the cost in such systems being attributed to the PSS support.

The main problem with using PSS supports revolves around operation during hydrogen separatrion. Since both the support material, and the membrane materials are metals, at temperatures above 275°C intermetallic diffusion will occur. Intermetallic diffusion is when molecules from the stainless steel support diffuse into the membrane layer and vice versa. The result is a drastic decrease in permeability, and potential compromise of membrane integrity due to the lattice structure of the membrane being changed. A common method for mitigating this effect is to modify the surface of the PSS support with an intermediate layer that is not susceptible to intermetallic diffusion. Common intermetallic diffusion barrier are zirconia, porous silica, and porous Pd-Ag. [34] It is also possible to create an oxide layer on the surface of the PSS support by heating the material to 80°C which achievges the same result. While these methods

are effective at mitigating the effects of intermetallic diffusion; they instead introduce a different problem where, in particular with some ceramic intermetallic diffusion layers, there is a difference in CTE between the material and support. Many of the intermetallic diffusion materials can also be made into supports on their own, at a much lower cost than PSS so it also opens the question of if these materials can be made into satisfactory supports on their own, why bother adding them to costly PSS supports.

Ceramic

Ceramic supports generally consist of porous ceramics manufactured through sintering of ceramic powders. They are a good candidate for supporting metallic membranes due to their uniform pore size distribution (0.1-10 µm) and their high chemical, thermal and mechanical stabilities.

While the materials and processes for manufacturing ceramic supports are cheaper, the overall manufacturing process requires more steps which increases the overall time required. The resulting membranes are also extremely brittle and can easily be damaged during handing.

Al_2O_3 has traditionally been the ceramic support of choice for palladium membranes however in recent years YSZ has become more popular. This is due to the increased mechanical stability of YSZ [127], and the fact that at higher temperatures aluminium can intrude into the active layer from the support through a mechanism similar to intermetallic diffusion.[34] Using ceramic supports solves the problem of intermetallic diffusion with the drawback of increasing the likelihood of delamination occurring due to different CTE values. Ceramic supports also have the advantage of being much cheaper to manufacture the metallic supports. [34]

Membrane deposition methods

There are various methods which can be used to deposit dense metal membranes onto the surface of a support can be carried through a wide number of chemical processes. From our reviews performed in sections 2.5.1 and 2.5.1 the most commonly used methods for deposition of dense metal membranes are PVD (e.g. magnetron sputterring) and ELP. Other methods including such as chemical vapour deposition (CVD) [128, 129, 130], electroplating deposition, atmospheric plasma [131] and spray pyrolisis [132] exist, however they have been omitted due to the inconsistency in final material, unreliability of the method, or cost. Additionally methods used to manufacture self-supporting membranes will not be discussed.

Chemical vapour deposition (CVD)

CVD involves the thermal composition of one or more metal complexes with a high volatility and subsequent deposition through nucleation and on a surface. Commonly used precursor materials are metal carbonyls or organometallic compoints. The method is known for it's ability to reliably deposit thin dense membrane layers typically (<2

µm). The method is held back by it's high material costs and the expensive operating conditions reaquired.[128, 133]

Physical vapour deposition (PVD)

PVD is a coating method in which a solid material, usually a pure metal, is vaporized in a vacuum system in the presence of a inert gas. The generated atoms migrate in all directions and condensate when coming in contact with a lower temperature substrate, forming a metallic film. PVD involves a using the desired membrane material as a target', and a 'coating surface' which in the case of membrane fabrication is the support. [134] The target is bombarded with ions or neutral particles which atomise the material. The inert gas, normally argon, is introduced to the sputtering chamber. The sputtering gas is ionized with a positive charge, while the target is subjected to a negative voltage typically around the magnitude of -300V. This potential difference causes the positively charged ions to impact the surface of the target, as this occurs atoms of the target material are removed and are intended to land on the substrate with enough energy to form a thin, dense, and strongly attached film. Magnetrons are commonly employed in sputtering which use magnetic fields to confine the charged plasma particles as close to the target as possible, which increases the sputter yield.

PVD in the form of Magnetron Sputtering is already an industrially widespread deposition method and is used to deposit metallic films for several applications and products. [134] The method can be used to deposit any metal or alloy. This technique can produce extremely thin nanostructured membrane layers while allowing the alloy composition to be accurately controlled and minimising the presence of impurities. [135, 136] However this method can prove to be expensive and complicated when looking to achieve defect free membranes. [137] The quality of the support is also a limiting factor with this fabrication method, the substrate must be extremely smooth in order for the film to properly adhere to the surface. In addition to this some problems arise due to the small grain sizes created by this technique which can cause grain growth and phase transitions at temperatures as low as 200°C. [138]

Electroplating deposition

EDP is a simple coating process where a thin metal layer is deposited on a substrate by the reduction of metal ions in solution. An electrical potential promotes the transport of the ions through the plating bath on to the desired support material which acts as a cathode. The thickness of the membrane is normally controlled by the electroplating time and the composition of the plating solution. The electrochemical process is simple and only involves simple and low-cost equipment. However, the support must be conductive, which greatly limits your choice. [128, 31].

Electroless Plating (ELP)

ELP is an autocatalytic deposition method in which a surface is coated with a metallic film through a two step process. The first step, normally referred to as the activation

step, involves preparing the surface by depositing small amounts of a metal with an equal to or higher electropositivity than the metal you desire onto the surface of the support material. Palladium is commonly used as the seeding material since it has the highest electroposity of metals capable of being deposited threough ELP and hence can be used to catalyse the deposition of any other metallic species. [139] The second step is metallization where the reduction/oxidation reactions occur, catalysed by the deposited seeds and initiated by a reducing agent added to the plating bath.

The activation step is required for all non conductive support materials (i.e. ceramics, glass) otherwise the chemical activity of support will be too low and plating will likely be inefficient or will fail. The most common method used is the stannum route which involves immersing the desired support in an acidic solution of $SnCl_2$, and subsequent immersion in a solution of the desired seeding metal in the form of a salt (chloride, nitride). The Sn^{2+} ions are adsorbed on the surface of the substrate in a hydrolytic form. The Sn^{2+} ions are then oxidised and replaced with Pd seeds. [139] The process for seeding a support with palladium is shown in equation 2.22 [139].

$$Sn^{2+}(aq) + Pd^{2+}(aq) \rightarrow Sn^{4+}(aq) + Pd(s) \tag{2.22}$$

The matalization or plating step involves placing the activated support material in a bath of a solution containing a metal source, such as a metallic salt, a complexion agent which stabilizes the metallic ions in the solution, and a stabilizing agent which regulates the pH of the palting bath. The bath is heated to the desired plating conditions before additon of a reducing agent which releases electrons and initiates the reaction. As the reaction proceeds metal is continuously deposited on the seed material, growing until eventually a dense, homogenous layer is formed.

Only a select number of metals can be deposited through electroless plating, these are shown in figure 2.7. [139] These metals can be deposited through electroless plating since they have a high reduction activity. While this is commonly seen as a disadvantage, in practice many of the metals were discussed in section 2.5.1 as having advantageous effects on the final membrane, and therefore is not as much of a hindrance as often reported. [139] This method also has the advantages of being extremely cheap, easy to perform, can be used to deposit on practically any geometry imaginable, and easily scalable. Due to the nature of this deposition method it is difficult to control the deposition rate and hence the thickness of the membrane deposited. This becomes an even larger problem when plating alloys as the final composition can be difficult to control has a large effect on the properties of the final membrane. Due to the nature of this deposition method the membranes are also susceptible to impurities which may have been present in the plating solutions or entered the solution in other means.

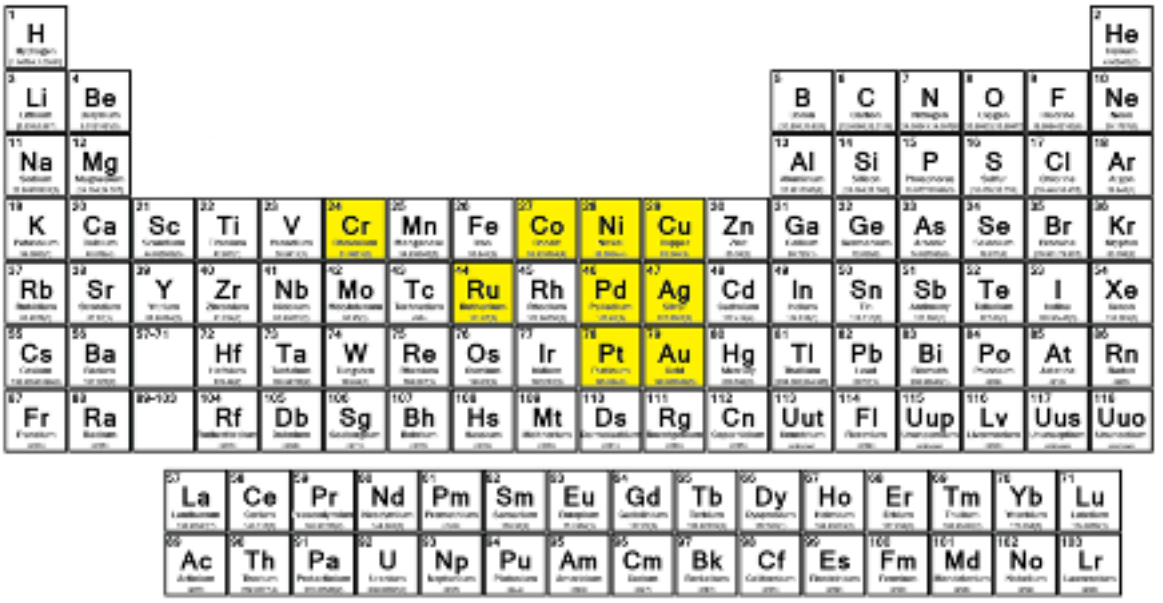

Figure 2.7: Metals which can be deposited using electro less plating [139]

There are two reported ways of creating palladium alloys through electroless plating; co-plating, and sequential plating. Co-plating has only been reported for Pd-Ag alloys since both palladium and silver have the same reducing agent.[140, 125] Co-plating may seem like the optimal manufacturing method since it cuts down on the number of steps required it is generally unsuitable for membrane production since the silver content of the bath must be lowered to at least 7% in order to prevent dendritical growth, and even then it is difficult to achieve a defect free layer while maintaining plating bath stability. [139]

Sequential plating involves plating layers on top of each other and forming thge alloy in a subsequent step. For example if a Pd-Ag membrane is desired a palladium layer would first be plated followed by a silver layer. [139] The membrane would then be annealed under a high temperature in order to achieve a homogeneous alloy.

2.6 Density functional theory for screening of membrane alloy compositions

Density functional theory (DFT) is a computationa quantum mechanical modelling method which is used to investigate the electronic structure of many body systems, in particular that of atoms, molecules and condensed phases. The method operates by providing an approximate solution to the Schrödinger equation of many body systems. This allows for prediction and calculation of material behaviour based purely on quantum mechanics, eliminating the need for fundamental material properties or experimental data. DFT techniques evaluate the electronic structure of a system by assuming a potential is acting on each of the systems electrons.

DFT-based methods prove to be useful in applications where a large number of elements and compositions must be investigated to optimize the desired material. For our application DFT calculations can be theoretically used to investigate, and quickly screen the suitability of any atomic configuration in the periodic table in combination with any of the ISO 14687-2 impurities. Much of the work in DFT screening of palladium membranes has been performed by the group of David S. Scholl who have suggested 5 criteria to ensure the application of DFT to the field of palladium membranes are performed in an optimal manner.[141], [142] These five criteria are:

1. The timescale and/or cost for predictions made using DFT should be shorter than it would take to perform the same tests experimentally
2. There should be minimal input from experimental data
3. Predictions must be made on propreties relevant to the end-use application
4. Quantitative data should be suffieicnt to make confident judgements on whether a material is promising or unpromising
5. The drawbacks and assumptions associated with DFT should be clearly stated to allow judgement on the predictions impact on real-world situations

This section will provide a a brief overview into DFT. This will include the key concepts required to perform DFT, different assumptions which can be made along with their advantages and disadvantages, and how these relate to our chosen application, screening of metal alloy membranes. Previous work relating to the use of DFT to predict the performance of palladium alloy membranes will be discussed and finally we will tie our planned work back to Scholl's criteria.

2.6.1 Key concepts

Simulating crystalline structures

DFT is focused on applying calculations to arrangements of atoms that are periodic in space. DFT calculations achieve this by defining the shape of the 'cell' which will be repeated periodically in space. [143]

In crystalline solids, which this thesis will focus on, the atoms are arranged in a periodic fashion which repeats after a certain length. In order to explain the crystal structure in this manner a concept called 'reciprocal space' or 'k space' is used. Using this concept planes can be defined as having coordinates within a crystal lattice. These coordinates are referred to as k-points and allow for the structure of a system to be calculated and therefore solved to it's lowest energy state. [143]

The most effective and widespread solution was developed by Monkhorst and Pack which is implemented into most DFT packages, allowing users to simply define the number of k-points in each direction of reciprocal space. Frequently the same number of k-points are used in each direction. [144]

The number of k-points used is important to the accuracy of the performed calculation, however higher k-points involve a larger number of calculations across the supercell in reciprocal space and therefore will result in higher calculation times for the whole system. [144] Convergence is often used to find the optimal number of k-points. This concept is visualised in figure 2.8

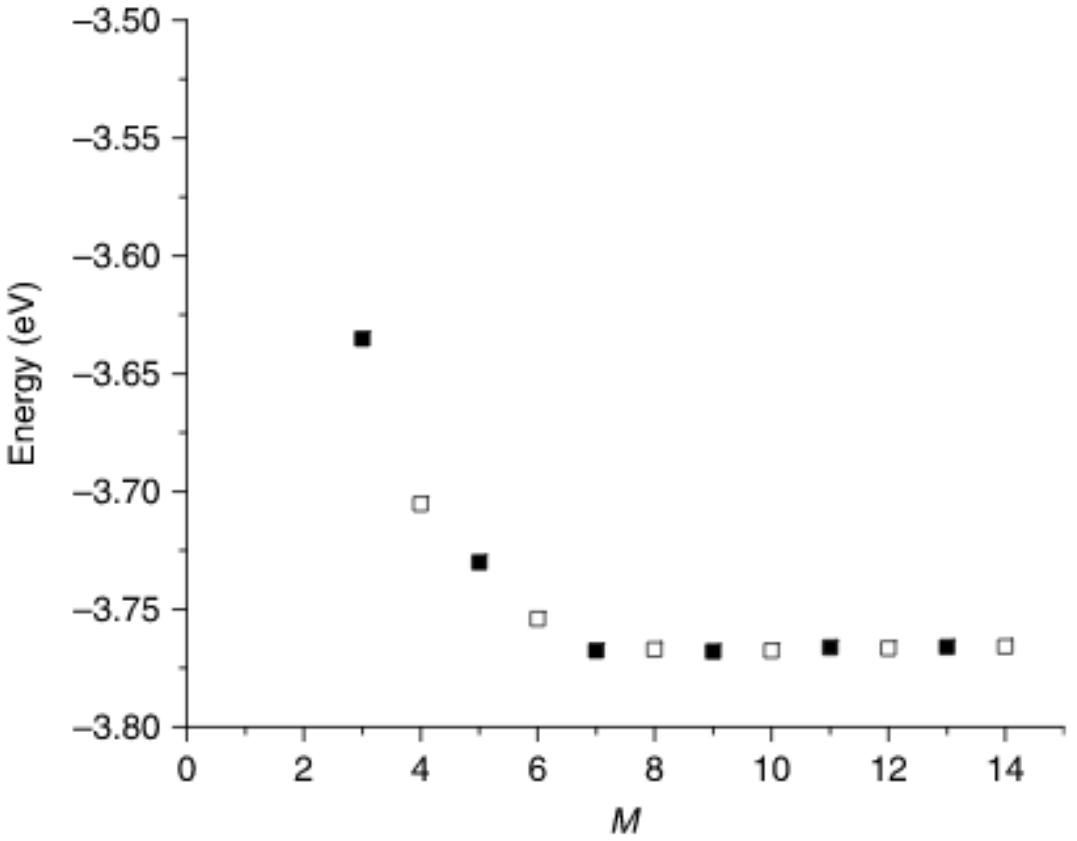

Figure 2.8: Total energies (per atom) for bulk Cu calculated as a function of M for calculations using MxMxM kpoints [144]

At lower numbers of k-points the total energy of the system is dependent on the number of k-points used. This value eventually converges and at M>8 k-points becomes completely independent of the nukmber of k-points used. This should be kept in mind when optimising the output values for any simulated system. K-points can be thought of as sampling points within a defined supercell. [143]

Defining the supercell which will be repeated in periodic space is a simple process and involves defining the volume for the supercell, along with the number, and position of the atoms residing within.

Metals are a special case in DFT and require the use of special algorithms to ensure that the energy state of a metallic system can be calculated without a high number of k-values. The two best methods for doing this are the tetrahedron method, or smearing.

The tetrahedron method involves defining a tertahedron using a discrete set of k-points. This tertahedron fills the reciprocal space and can be integrated to form at all points in the k space and evaluated. [143]

Smearing involves forcing the function to be continuously integrated to replace any step functions with a smoother function. Ideally the result of the calculation should be a result which can be extrapolated to the limit where smearing is eliminated. [143]

When simulating a membrane often a slab geometry is used in order to avoid 'edge effects' where simulation results are skewed because of unique surface boundaries resulting from being at the edge of a supercell. The geometry of such a model is achieved through the generation of a box containing a multilayer atomic slab representing the membrane material with a vaccum layer in the remaining volume. From literature palladium membranes are normally in the fcc material phase [145] (with the exception being $Pd_{40}Cu_{60}$ which is in the bcc phase). It is common to represent this using 3-5 atomic layers of palladium. To create alloys random atoms can be substituted for other elements to achieve the desired alloy composition.

In order to determine the adsorption energy of impurities on a palladium membrane using DFT both the slab being used to represent the membrane surface, and the individual gas molecule must first be simulated in order to determine their individual ground energy states. Then the gas molecule must be adsorbed onto the surface of the membrane. In a crystalline structure there are often multiple sites which are avaliable for gas adsorption. In an fcc structure such as Pd there are 4 main sites which can be considered, shown in figure 2.9 [146]. Once the site is chosen the simulation is iterated, slightly changing the distances between molecules until the mininum ground state is found and therefore the ground energy level of the system composed of the palladium membrane, and the adsorbed impurity. The adsorption energy, $E_{i_{ads}}$, for the adsorption of a gaseous impurity on the surface is calculated equation 2.23. Where E_{slab+i} is the total energy of the relaxed gas-surface system where i is the simulated gas, E_slab and E_i are the total energy of relaxed bare surface and gas molecule respectively. Since a system will always tend towards it's lowest energy state, if the total energy of the $E_{i,ads}$ is lower than the sum of it's component energies, it indicates an affinity for the target impurity to adsorb onto the surface of the membrane.

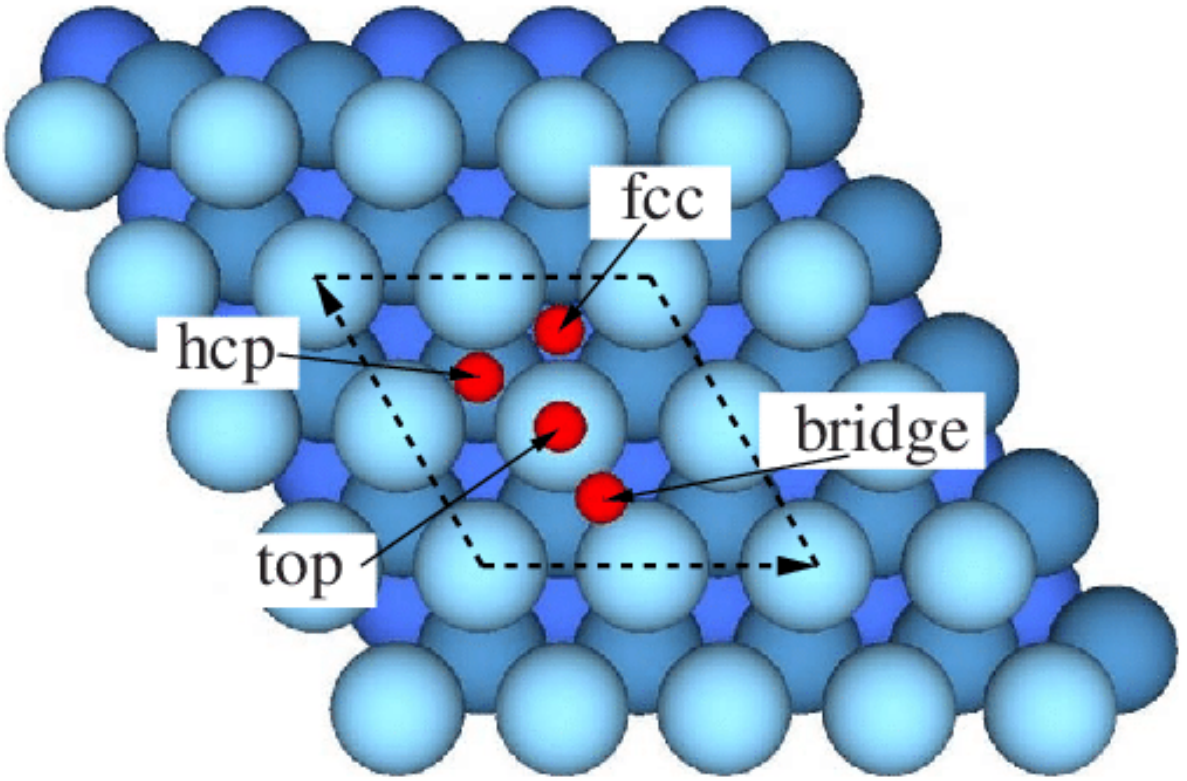

Figure 2.9: Top view of the high-symmetry adsorption sites fcc, hcp, bridge, and top [146]

$$E_{i,ads} = E_{slab} + E_i - E_{slab+i} \tag{2.23}$$

Approximations

The ultimate goal of DFT is to calculate the ground-state energy of the defined system. This was shown by Kohn, Holberg and Sham who discovered that this could be found by finding a self-consistent solution to a set of single particle equations, as an exchange correlation. A major complication to this however is that a gaurenteed exchange correlation function simply does not exist, therefore they must be approximated. Two common methods for approximating exchange correlations are local density approximation (LDA) and generalized gradient approximation (GGA)

LDA is where the energy of the system is assumed to depend on the electron density. LDA is able to predict the energy of a structure to within 1-2% of the experimental value. Unfortunately the method fails when looking to predict magnetic properties of materials and the band gaps calculated generally tend to overshoot the bond strengths. [147]

GGA is an improvement over LDA and takes into account the gradient of electron density as well ad the average electron density. This adds an extra layer of computational complexity. it allows for strucural properties to be predicted to within 1% of the experimental values and the total energy to be calculated to 1 kJ/mol. [147] This is also claimed in literature [148].

This thesis will mainly focus on the solid state chemistry in the bulk of the material. For this reason GGA functionals have been chosen as they been shown in numerous publications to perform well.

Pseudopotentials

A pseudopotential is a method used to replace the electron density of a chosen set of core electrons in an atom with a smoothed density chosen to match the physical and mathematical properties of the ionic core of the atom. [147] The use of a pseudopotential is extremely important in reducing computational burden by reducing the number of planes calculated within the atom. This is commonly referred to as the 'frozen core' assumption whereby only the behaviour of the outer most electrons are calculated, and the inner electrons, whose behaviour has previously been calculated, is considered fixed. [147]

The main differentiating feature between different tyupes of pseudopotentials is the mininum energy cutoff for each atom in an equation. The mioninum energy cutoff value refers to the number of plane wave functions which will be used to represent the system, a higher cutoff value means that more plane wave functions are used to represent the bahviour of electrons. The most commonly used pseudopotentials are ultrasoft pseudopotentials which feature a relatively low energy cutoff, making them extremely computationally efficient. A disadvantage of using an ultrasoft pseudopotential is that they require the use of empirical values in defining the properties of the core. However a review of various types of pseudopotentials found that there is virtually no difference in results regardless of what pseudopotential is used and this only becomes a factor whern more complex phenomena such as magnetic properties have to be considered. [147]

Calculations that do not use a pseudopotential are called 'all electron' calculations. However their use is limited due to increased computational burden. [147]

2.6.2 Use cases, and limitations

Most work revolving around the use of DFT to predict the adsorption strength of impurities on palladium and palladium alloy surfaces has focused on catalysis of chemical reactions. As a result there are a limited number of papers focusing on quantifying the interaction between these key hydrogen impurities and membranes. Papers which use DFT to predict the behaviour of hydrogen impurities on the surface of palladium membranes are shown in table 2.7 . The most relevant study performed by Ozdogan et al [149] studied the effect of H_2 and H_2S adsorption energies when small additions of Cu and Nb were added to the membrane composition. The results indicated that while the addition of Cu and Nb hindered hydrogen adsorption, they had a large effect on the

adsorption ennergy of H_2S, concluding that Nb has a higher affinity for H_2S compared to Pd and a lower addinity for Cu. The results were correlated with experimental results and found to be within 1% error which is consistent with results found from using GGA.

Another useful study from Herron et al [150] studied the adsorption of a variety of atomic species (H, O, N, S, and C), molecular species (N_2, HCN, CO, NO, and NH_3), and molecular fragments (CN, NH_2, NH, CH_3, CH_2, CH, HNO, NOH, and OH) on the face of Pd(111) to quantify it's effectivness at catalysing a variety of industrial reactions. Depsite it's target application not being membranes, the results are still relevant to our desired study since a number of the molecular species and molecular fragments tested can be expected to be found in hydrogen. As well as quantifying the binding enmergies of all these molecules, the potential energies also indicated that the only reaction thermochemically preferable is the decomposition of NO. Which gives further evidence that reactions such as water gas shift occuring during catalysis are of no concern.

Outside of these the technique has seen use in predicting the stability of palladium and palladium alloy membranes. A number of studies have successfully combined data from density functional theory to calculate the solubility, diffusivity and permeability of PdCu ([151], [152], [153]), PdAg([154], [155], [156]), PdAu([154], [155], [156]), and ternary alloy ([157], [158],[159] membranes. In particular the study by Morreale et al showed that DFT can be used predict experimental data, although to a limited degree as experimental results were approximately 7 times greater than simulated results. [72]. The greatest challenge when attempting to describe the permeation of hydrogen through metallic membranes is frequent disordering of atoms during the simulation runtime, throwing off results. Other methods such as cluster expansion have been employed in order to overcome this.

The fundamental limitation of using DFT to accurately predict the behaviour of materials is that ultimately such calculation usually calculate, at a maxinum, interactions between 10-30 of atoms at a time. This is in no way similar to a physical system where the number of atoms is likely to be in the millions.[147]It must be understood that DFT calculations draw results from extremely small numbers of atoms, and while relevant to phsycal systems, are likely to result in some errors because of this. [147]

DFT is also known to be inaccurate in describing systems where weak van der walls attractions exist between molecules and atoms. [147] This is due to the fact that such attractions are a result of temporary fluctuations in electron density. In order to describe the effect of these interactions on a quantum mechanic level it is necessary to use high level wave function based methods which DFT is unable to accuratly predict. This explains why research only focuses on predicting one molecule on a surface at a time, while multiple molecules could theoretically be placed in a simulation, due to the lack of intermolecular forces being taken into account such results are likely to be innacurate. [147]

Despite these drawbacks DFT analysis is a useful tool for screening of potential palladium alloy membrane. The technique is capable of speeding up material development by eliminating options that are unlikelym to work, cutting down on trial and error. Due to inacuracies in the technique however it is unlikely that it will ever become a stan-

dalone technique in membrane research and it's findings should always be backed up by experimental data.

Table 2.7: Review of DFT studies for adsorption of ISO 14687-2 impurites and hydrogen on palladium membrane surfaces

Simulated material	Structure	Approximation	Exchange function	K-points	Adsorbed species	Adsorption site	Binding energy (eV)	ref
Pd	4x4x4 unit cell	GGA	PW91	5x5x1	H_2	hcp	- 0.5485	[149]
Pd	4x4x4 unit cell	GGA	PW91	5x5x1	H_2	fcc	- 0.5927	[149]
Pd	4x4x4 unit cell	GGA	PW91	5x5x1	H_2S	bridge-fcc-top (H-H-S)	- 0.7	[149]
Pd	4x4x4 unit cell	GGA	PW91	5x5x1	H_2S	bridge-bridge-top (H-H-S)	- 0.707	[149]
Pd	4x4x4 unit cell	GGA	PW91	5x5x1	H_2S	bridge-hcp-top (H-H-S)	- 0.707	[149]
Pd	4x4x4 unit cell	GGA	PW91	5x5x1	H_2S	fcc-hcp-top (H-H-S)	- 0.692	[149]
$PdNb_{1.6}$	4x4x4 unit cell	GGA	PW91	5x5x1	H_2	hcp	-0.4259	[149]
$PdNb_{1.6}$	4x4x4 unit cell	GGA	PW91	5x5x1	H_2	fcc	-0.4740	[149]
$PdNb_{1.6}$	4x4x4 unit cell	GGA	PW91	5x5x1	H_2S	bridge-fcc-top (H-H-S)	- 0.803	[149]
$PdNb_{1.6}$	4x4x4 unit cell	GGA	PW91	5x5x1	H_2S	bridge-bridge-top (H-H-S)	- 0.704	[149]
$PdNb_{1.6}$	4x4x4 unit cell	GGA	PW91	5x5x1	H_2S	bridge-hcp-top (H-H-S)	- 0.735	[149]
$PdNb_{1.6}$	4x4x4 unit cell	GGA	PW91	5x5x1	H_2S	fcc-hcp-top (H-H-S)	- 0.682	[149]
$PdNb_{1.6}$	4x4x4 unit cell	GGA	PW91	5x5x1	H_2S	hcp-bridge-top (H-H-S)	- 0.602	[149]
$PdCu_{1.6}$	4x4x4 unit cell	GGA	PW91	5x5x1	H_2	hcp	-0.4946	[149]
$PdCu_{1.6}$	4x4x4 unit cell	GGA	PW91	5x5x1	H_2	fcc	-0.5357	[149]
$PdNb_{1.6}$	4x4x4 unit cell	GGA	PW91	5x5x1	H_2S	bridge-fcc-top (H-H-S)	- 0.429	[149]
$PdNb_{1.6}$	4x4x4 unit cell	GGA	PW91	5x5x1	H_2S	bridge-hcp-top (H-H-S)	- 0.431	[149]
Pd	2x2x4 unit cell	GGA	PW91	3x3x1	N_2	top	- 0.23	[150]
Pd	2x2x4 unit cell	GGA	PW91	3x3x1	N_2	fcc	- 0.02	[150]
Pd	2x2x4 unit cell	GGA	PW91	3x3x1	N_2	bridge	- 0.07	[150]
Pd	2x2x4 unit cell	GGA	PW91	3x3x1	NH_3	top	- 0.62	[150]
Pd	2x2x4 unit cell	GGA	PW91	3x3x1	NH_2	top	-1.63	[150]
Pd	2x2x4 unit cell	GGA	PW91	3x3x1	NH_2	bridge	-2.15	[150]
Pd	2x2x4 unit cell	GGA	PW91	3x3x1	NH	fcc	-3.45	[150]
Pd	2x2x4 unit cell	GGA	PW91	3x3x1	NH	hcp	-3.30	[150]

Pd	2x2x4 unit cell	GGA	PW91	3x3x1	CO	top	-1.29	[150]
Pd	2x2x4 unit cell	GGA	PW91	3x3x1	CO	fcc	-1.95	[150]
Pd	2x2x4 unit cell	GGA	PW91	3x3x1	CO	hcp	-1.96	[150]
Pd	2x2x4 unit cell	GGA	PW91	3x3x1	CO	bridge	-1.77	[150]
Pd	2x2x4 unit cell	GGA	PW91	3x3x1	CH_3	top	-1.67	[150]
Pd	2x2x4 unit cell	GGA	PW91	3x3x1	CH_2	bridge	-3.56	[150]
Pd	2x2x4 unit cell	GGA	PW91	3x3x1	CH	fcc	-5.91	[150]
Pd	2x2x4 unit cell	GGA	PW91	3x3x1	CH	hcp	-5.89	[150]
Pd	2x2x4 unit cell	GGA	PW91	3x3x1	CH	hcp	-5.89	[150]
Pd	2x2x3 unit cell	GGA	PW91	3x3x1	H_2	top	-0.07	[148]
Pd	2x2x3 unit cell	GGA	PW91	3x3x1	H_2	bridge	-0.37	[148]
Pd	2x2x3 unit cell	GGA	PW91	3x3x1	H_2	fcc	-0.49	[148]
Pd	2x2x3 unit cell	GGA	PW91	3x3x1	H_2	hcp	-0.45	[148]
$PdAg_{25}$	2x2x3 unit cell	GGA	PW91	3x3x1	H_2	top	0.84	[148]
$PdAg_{25}$	2x2x3 unit cell	GGA	PW91	3x3x1	H_2	bridge	-0.27	[148]
$PdAg_{25}$	2x2x3 unit cell	GGA	PW91	3x3x1	H_2	fcc	-0.22	[148]
$PdAg_{25}$	2x2x3 unit cell	GGA	PW91	3x3x1	H_2	hcp	-0.22	[148]

2.7 Conclusion

This chapter provided a review of the hydrogen process, from how hydrogen is produced and it's relationship to the impurites which can end up in the supply chain. The effect of these impurities on the operation of a fuel cell electric vehicle was discussed and the liklihood of these impurities reaching a consumers fuel cell.

Different methods for enriching hydrogen was discussed with one of the most promising methods identified being hydrogen impurity enrichment using a dense metal membrane. From here a number of membrane materials designed to separate hydrogen from multicomponent mixtures. An extensive summary has been provided on the separation performance and stability of these materials with an emphasis on the complications related to transitioning the use of these materials from laboratory and R&D efforts, to industrially relevant processes. The key observation is that while there is a large research focus on new membrane materials, there is a lack of research looking into the engineering of these membranes into functional systems and products. Out of the hundreds of materials being researched for gas separation, commercially only four-eight different polymers are being used, with some niche applications using palladium membranes. Research focus should shift towards focusing on repeatability, scale up, and creating engineered systems where new membrane materials can be used in order to make progress in bringing these new materials to market. Out of the membrane materials reviewed palladium based alloys were the most appropriate to be used for hydrogen impurity enrichment and focus in this thesis will be to find a suitable composition for measuring ISO 14687-2 impurities while minimising interaction with reactants.

DFT based theories were discuessed and identified as a method to save time money and cost when attemtping to optimise the palladium alloy composition. There is a gap in research on using this technique for palladium alloys specifically targeting ISO 14687-2 impurities. While limited literature exists since many papers adress the use of palladium surfaces as catalysts the research is useful for creating a starting base. Palladium alloy membranes can be screened for materials which exhibit the lowest reactivity with ISO 14687-2 impuruties, and once identified, they can be manufactured and tested. It is important to note however that there are a number of innacuracies involved in the technique and should only be used as a rough guide.

References

[1] Sangeetha Dharmalingam, Vaidhegi Kugarajah, and Moogambigai Sugumar. Chapter 1.7 - Membranes for Microbial Fuel Cells. In S Venkata Mohan, Sunita Varjani, and Ashok B T Microbial Electrochemical Technology Pandey, editors, *Biomass, Biofuels and Biochemicals*, pages 143–194. Elsevier, 2019. ISBN 978-0-444-64052-9. doi: https://doi.org/10.1016/B978-0-444-64052-9.00007-8. URL `http://www.sciencedirect.com/science/article/pii/B9780444640529000078`.

[2] A Alaswad, A Palumbo, M Dassisti, A G B T Reference Module in Materials Science Olabi, and Materials Engineering. Fuel Cell Technologies, Applications, and State of the Art. A Reference Guide. Elsevier, 2016. ISBN 978-0-12-803581-8. doi: https://doi.org/10.1016/B978-0-12-803581-8.04009-1. URL `http://www.sciencedirect.com/science/article/pii/B9780128035818040091`.

[3] Viral Mehta and Joyce Smith Cooper. Review and analysis of PEM fuel cell design and manufacturing. *Journal of Power Sources*, 114(1):32–53, 2003. ISSN 0378-7753. doi: https://doi.org/10.1016/S0378-7753(02)00542-6. URL `http://www.sciencedirect.com/science/article/pii/S0378775302005426`.

[4] Zhongliang Li, Zhixue Zheng, Liangfei Xu, and Xiaonan Lu. A review of the applications of fuel cells in microgrids: opportunities and challenges. *BMC Energy*, 1, dec 2019. doi: 10.1186/s42500-019-0008-3.

[5] Klaus-Michael Mangold. Introduction to Hydrogen Technology.By Roman J. Press, K. S. V. Santhanam, Massoud J. Miri, Alla V. Bailey, and Gerald A. Takacs. *ChemSusChem*, 2(8):781, aug 2009. ISSN 1864-5631. doi: 10.1002/cssc.200900109. URL `https://doi.org/10.1002/cssc.200900109`.

[6] J D Holladay, J Hu, D L King, and Y Wang. An overview of hydrogen production technologies. *Catalysis Today*, 139(4):244–260, 2009. ISSN 0920-5861. doi: https://doi.org/10.1016/j.cattod.2008.08.039. URL `http://www.sciencedirect.com/science/article/pii/S0920586108004100`.

[7] International Energy Agency (IEA). Technology Roadmap Hydrogen and Fuel Cell. Technical report, IEA/OECD Paris., 2015.

[8] N Muradov. 17 - Low-carbon production of hydrogen from fossil fuels. In Velu Subramani, Angelo Basile, and T Nejat B T Compendium of Hydrogen Energy Veziroğlu, editors, *Woodhead Publishing Series in Energy*, pages 489–522. Woodhead Publishing, Oxford, 2015. ISBN 978-1-78242-361-4. doi: https://doi.org/10.1016/B978-1-78242-361-4.00017-0. URL http://www.sciencedirect.com/science/article/pii/B9781782423614000170.

[9] Hydrogen Council. Path to hydrogencompetitiveness a cost perspective. Jan 2020.

[10] Shakeel Ahmed, Abdullah Aitani, Faizur Rahman, Ali Al-Dawood, and Fahad Al-Muhaish. Decomposition of hydrocarbons to hydrogen and carbon. *Applied Catalysis A: General*, 359(1):1–24, 2009. ISSN 0926-860X. doi: https://doi.org/10.1016/j.apcata.2009.02.038. URL http://www.sciencedirect.com/science/article/pii/S0926860X09001719.

[11] Nazim Z Muradov and T Nejat Veziroğlu. "Green" path from fossil-based to hydrogen economy: An overview of carbon-neutral technologies. *International Journal of Hydrogen Energy*, 33(23):6804–6839, 2008. ISSN 0360-3199. doi: https://doi.org/10.1016/j.ijhydene.2008.08.054. URL http://www.sciencedirect.com/science/article/pii/S036031990801118X.

[12] Canan Acar and Ibrahim Dincer. Comparative assessment of hydrogen production methods from renewable and non-renewable sources. *International Journal of Hydrogen Energy*, 39(1):1–12, 2014. ISSN 0360-3199. doi: https://doi.org/10.1016/j.ijhydene.2013.10.060. URL http://www.sciencedirect.com/science/article/pii/S0360319913025330.

[13] C Koroneos, A Dompros, G Roumbas, and N Moussiopoulos. Life cycle assessment of hydrogen fuel production processes. *International Journal of Hydrogen Energy*, 29(14):1443–1450, 2004. ISSN 0360-3199. doi: https://doi.org/10.1016/j.ijhydene.2004.01.016. URL http://www.sciencedirect.com/science/article/pii/S0360319904000655.

[14] Energy & Industrial Strategy Department for Business. Prices of fuels purchased by non-domestic consumers in the united kingdom excluding/including ccl (qep 3.4.1 and 3.4.2). Mar 2020. URL https://www.gov.uk/government/statistical-data-sets/gas-and-electricity-prices-in-the-non-domestic-sector.

[15] Argonne National Lab. Life cycle greenhouse gas emissions of by-product hydrogen from chloro-alkali plants. Dec 2017.

[16] David A. Nelson. Chemical process industries (shreve, r. norris; brink, joseph a.). *Journal of Chemical Education*, 57(9):A270, 1980. doi: 10.1021/ed057pA270.1. URL https://doi.org/10.1021/ed057pA270.1.

[17] Hussam Khasawneh, Motasem N Saidan, and Mohammad Al-Addous. Utilization of hydrogen as clean energy resource in chlor-alkali process. *Energy Exploration & Exploitation*, 37(3):1053–1072, 2019. doi: 10.1177/0144598719839767. URL https://doi.org/10.1177/0144598719839767.

[18] Thomas Bacquart, Arul Murugan, Martine Carré, Bruno Gozlan, Fabien Auprêtre, Frédérique Haloua, and Thor A Aarhaug. Probability of occurrence of ISO 14687-2 contaminants in hydrogen: Principles and examples from steam methane reforming and electrolysis (water and chlor-alkali) production processes model. *International Journal of Hydrogen Energy*, 43(26):11872–11883, 2018. ISSN 0360-3199. doi: https://doi.org/10.1016/j.ijhydene.2018.03.084. URL http://www.sciencedirect.com/science/article/pii/S0360319918308450.

[19] International Standard ISO 14687-2: 2012. Hydrogen Fuel - Product Specification, 2012.

[20] Enrico Doná, Michael Cordin, Clemens Deisl, Erminald Bertel, Cesare Franchini, Rinaldo Zucca, and Josef Redinger. Halogen-Induced Corrosion of Platinum. *Journal of the American Chemical Society*, 131(8):2827–2829, mar 2009. ISSN 0002-7863. doi: 10.1021/ja809674n. URL https://doi.org/10.1021/ja809674n.

[21] Shabbir Ahmed, Sheldon H D Lee, and Dionissios D Papadias. Analysis of trace impurities in hydrogen: Enrichment of impurities using a H2 selective permeation membrane . *International Journal of Hydrogen Energy*, 35(22):12480–12490, 2010. doi: 10.1016/j.ijhydene.2010.08.042.

[22] Arul Murugan and Andrew S Brown. Advancing the analysis of impurities in hydrogen by use of a novel tracer enrichment method. *Analytical Methods*, 6(15): 5472, 2014. doi: 10.1039/c3ay42174k.

[23] Arul Murugan and Andrew S Brown. Review of purity analysis methods for performing quality assurance of fuel cell hydrogen. *International Journal of Hydrogen Energy*, 40(11):4219–4233, 2015. doi: 10.1016/j.ijhydene.2015.01.041.

[24] Peter R Bossard, Jacques Mettes, Luis Breziner, and Emeritus Fred Gornick. New Sensor for Measuring Trace Impurities in Ultra Pure Hydrogen. *Power & Energy, USA*.

[25] Jürgen Hille. Enrichment and mass spectrometric analysis of trace impurity concentrations in gases. *Journal of Chromatography A*, 502:265–274, 1990. ISSN 0021-9673. doi: https://doi.org/10.1016/S0021-9673(01)89591-1. URL http://www.sciencedirect.com/science/article/pii/S0021967301895911.

[26] A Volkov. Membrane Compaction. In Giorno L Drioli E., editor, *Encycolpedia of Membranes*. Springer, Berlin, Heidelberg, 2014.

[27] A. Gugliuzza. Membrane Swelling. In Drioli E. and Giorno L., editors, *Encyclopedia of Membranes*. Springer, Berlin, Heidelberg, 2015.

[28] R. Farrauto, S. Hwang, L. Shore, W. Ruettinger, J. Lampert, T. Giroux, Y. Liu, and O. Ilinich. New Material Needs for Hydrocarbon Fuel Processing: Generating Hydrogen for the PEM Fuel Cell. *Annual Review of Materials Research*, 33(1):1–27, 2003. ISSN 1531-7331. doi: 10.1146/annurev.matsci.33.022802.091348. URL `http://www.annualreviews.org/doi/10.1146/annurev.matsci.33.022802.091348`.

[29] K. Nagai, A. Higuchi, and T. Nakagawa. Gas permeability and stability of poly(1-trimethylsilyl-1-propyne-co-1-phenyl-1-propyne) membranes. *J. Polym. Sci.: Part B: Polym. Phys.*, 33:289, 1995.

[30] G. Polotskaya, M. Goikhman, I. Podeshvo, V. Kudryavtsev, Z. Pientka, L. Brozova, and M. Bleha. Gas transport properties of polybenzoxazinoneimides and their prepolymers. *Polymer*, 46(11):3730–3736, 2005. ISSN 00323861. doi: 10.1016/j.polymer.2005.02.111.

[31] Tina M Nenoff Nathan W. Ockwig. Membranes for Hydrogen Separation. *Chemical Reviews*, 107:4078–4110, 2007.

[32] Hong Joo Lee, Hiroyuki Suda, Kenji Haraya, and Seung Hyeon Moon. Gas permeation properties of carbon molecular sieving membranes derived from the polymer blend of polyphenylene oxide (PPO)/polyvinylpyrrolidone (PVP). *Journal of Membrane Science*, 296(1-2):139–146, 2007. ISSN 03767388. doi: 10.1016/j.memsci.2007.03.025.

[33] Huiyuan Gao, Y S Lin, Yongdan Li, and Baoquan Zhang. Chemical Stability and Its Improvement of Palladium-Based Metallic Membranes. *Ind. Eng. Chem. Res.*, 43:6920–6930, 2004.

[34] K Atsonios, K D Panopoulos, A Doukelis, A K Koumanakos, E Kakaras, T A Peters, and Y C van Delft. Introduction to palladium membrane technology. In A Doukelis, K Panopoulos, A Koumanakos, and E Kakaras, editors, *Palladium Membrane Technology for Hydrogen Production, Carbon Capture and Other Application*, pages 1–21. Woodhead Publishing, 2015. doi: 10.1533/9781782422419.1.

[35] Truls Norby and Reidar Haugsrud. Dense Ceramic Membranes for Hydrogen Separation, in Membranes for Energy Conversion. *Nonporous inorganic membranes*, pages 169–216, 2008. URL `http://books.google.com/books?hl=en{\&}lr={\&}id=gCQjw-cyulAC{\&}oi=fnd{\&}pg=PA1{\&}dq=Dense+Ceramic+Membranes+for+Hydrogen+Separation{\&}ots=e-3oiNW5EW{\&}sig=Iv9bFzwJWBTYe7brB66{\_}qQ5W{\_}u8`.

[36] D.H. Weinkauf and D.R. Paul. Gas transport properties of thermotropic liquid-crystalline copolyesters. II. The effects of copolymer composition. *J. Polym. Sci.: Part B: Polym. Phys.*, 30:837, 1992.

[37] Tina M Nenoff Nathan W. Ockwig. Membranes for Hydrogen Separation. *Chemical Reviews*, 107:4078–4110, 2007.

[38] V. Gryaznov. Metal Containing Membranes for the Production of Ultrapure Hydrogen and the Recovery of Hydrogen Isotopes. *Separation & Purification Reviews*, 29(2):171–187, 2000. ISSN 1542-2119. doi: 10.1081/SPM-100100008.

[39] N A Al-Mufachi, N V Rees, and R Steinberger-Wilkens. Hydrogen selective membranes: A review of palladium-based dense metal membranes. *Renewable and Sustainable Energy Reviews*, 47:540–551, 2015. doi: 10.1016/j.rser.2015.03.026.

[40] Johnson Matthey Precious Metals Management. Price Tables, 2016.

[41] Ted B Flanagan and W A Oates. The Palladium-Hydrogen System. *Annu. Rev. Mater. Sci*, 21:269–304, 1991.

[42] Hui Li, Hengyong Xu, and Wenzhao Li. Study of n value and α/β palladium hydride phase transition within the ultra-thin palladium composite membrane. *Journal of Membrane Science*, 324(1-2):44–49, 2008. doi: 10.1016/j.memsci.2008.06.053.

[43] M V Mundschau, X Xie, C R Evenson Iv, and A F Sammells. Dense inorganic membranes for production of hydrogen from methane and coal with carbon dioxide sequestration. *Catalysis today*, 118:12–23, 2006. doi: 10.1016/j.cattod.2006.01.042.

[44] Ying She, Sean C Emerson, Neal J Magdefrau, Susanne M Opalka, Catherine Thibaud-Erkey, and Thomas H Vanderspurt. Hydrogen permeability of sulfur tolerant Pd–Cu alloy membranes. *Journal of Membrane Science*, 452:203–211, 2014. doi: 10.1016/j.memsci.2013.09.025.

[45] M D Dolan. Non-Pd BCC alloy membranes for industrial hydrogen separation. *Journal of Membrane Science*, 362(1-2):12–28, 2010. doi: 10.1016/j.memsci.2010.06.068.

[46] Ekin Ozdogan Wilcox and Jennifer. Investigation of H2 and H2S Adsorption on Niobium- and Copper-Doped Palladium Surfaces. *J. Phys. Cherm. B*, pages 12851–12585, 2010. doi: 10.1021/acs.energyfuels.5b01294.

[47] I R Harris D.T. Hughes. A comparative study of hydrogen permeabilities and solubilities in some palladium solid solution alloys. *Journal of Less Common Metals*, 61:9–21, 1978.

[48] Casey P O Brien, Bret H Howard, James B Miller, Bryan D Morreale, and Andrew J Gellman. Inhibition of hydrogen transport through Pd and Pd47Cu53 membranes by H2S at 350C. *Journal of Membrane Science*, 349(1-2):380–384, 2010. doi: 10.1016/j.memsci.2009.11.070.

[49] A Kulprathipanja, G Alptekin, J Falconer, and J Way. Pd and Pd–Cu membranes: inhibition of H2 permeation by H2S. *Journal of Membrane Science*, 254(1-2):49–62, 2005. doi: 10.1016/j.memsci.2004.11.031.

[50] Chao-Huang Chen and Yi Hua Ma. The effect of H2S on the performance of Pd and Pd/Au composite membrane. *Journal of Membrane Science*, 362(1-2): 535–544, 2010. doi: 10.1016/j.memsci.2010.07.002.

[51] David L. McKinley. Metal Alloy for Hydrogen Separation and Purification, 1964.

[52] G. Roa, F., Thoen, P.M., Gade, S.K., Way, J.G., De Voss, S., and Alptekin. Palladium-Copper and Palladium-Gold alloy Composite membranes for hydrogen separations. In *Inorganic Membranes for Energy and Environmental Applications*, page 211. 2009.

[53] APMEX. Silver Prices, 2016. URL `http://www.apmex.com/spotprices/silver-prices`.

[54] Lixia Peng, Yongchu Rao, Lizhu Luo, and Chang'An Chen. The poisoning of Pd–Y alloy membranes by carbon monoxide. *Journal of Alloys and Compounds*, 486(1-2):74–77, 2009. doi: 10.1016/j.jallcom.2009.06.158.

[55] Kenneth J. Bryden and Jackie Y. Ying. Nanostructured palladium-iron membranes for hydrogen separation and membrane hydrogenation reactions. *Journal of Membrane Science*, 203(1-2):29–42, 2002. ISSN 03767388. doi: 10.1016/S0376-7388(01)00736-0.

[56] B. H. Howard and B. D. Morreale. Effect of H ₂ S on performance of Pd ₄ Pt alloy membranes. *Energy Materials*, 3(3):177–185, 2008. ISSN 1748-9237. doi: 10.1179/174892309X12519750237717. URL `http://www.tandfonline.com/doi/full/10.1179/174892309X12519750237717`.

[57] Sabina K. Gade, Sarah J. DeVoss, Kent E. Coulter, Stephen N. Paglieri, Gökhan O. Alptekin, and J. Douglas Way. Palladium-gold membranes in mixed gas streams with hydrogen sulfide: Effect of alloy content and fabrication technique. *Journal of Membrane Science*, 378(1-2):35–41, 2011. ISSN 03767388. doi: 10.1016/j.memsci.2010.11.044. URL `http://dx.doi.org/10.1016/j.memsci.2010.11.044`.

[58] Shin Kun Ryi, Anwu Li, C. Jim Lim, and John R. Grace. Novel non-alloy Ru/Pd composite membrane fabricated by electroless plating for hydrogen separation. *International Journal of Hydrogen Energy*, 36(15):9335–9340, 2011. ISSN 03603199. doi: 10.1016/j.ijhydene.2010.06.014. URL `http://dx.doi.org/10.1016/j.ijhydene.2010.06.014`.

[59] Kent E. Coulter, J. Douglas Way, Sabina K. Gade, Saurabh Chaudhari, Gökhan O. Alptekin, Sarah J. DeVoss, Stephen N. Paglieri, and Bill Pledger. Sulfur tolerant PdAu and PdAuPt alloy hydrogen separation membranes. *Journal of Membrane Science*, 405-406:11–19, 2012. ISSN 03767388. doi: 10.1016/j.memsci.2012.02.018. URL http://dx.doi.org/10.1016/j.memsci.2012.02.018.

[60] Fernando Braun, James B. Miller, Andrew J. Gellman, Ana M. Tarditi, Benoit Fleutot, Petro Kondratyuk, and Laura M. Cornaglia. PdAgAu alloy with high resistance to corrosion by H2S. *International Journal of Hydrogen Energy*, 37(23): 18547–18555, 2012. ISSN 03603199. doi: 10.1016/j.ijhydene.2012.09.040. URL http://dx.doi.org/10.1016/j.ijhydene.2012.09.040.

[61] Fernando Braun, Ana M Tarditi, James B Miller, and Laura M Cornaglia. Pd-based binary and ternary alloy membranes: Morphological and perm-selective characterization in the presence of H2S. *Journal of Membrane Science*, 450:299–307, 2014. doi: 10.1016/j.memsci.2013.09.026.

[62] T. A. Peters, T. Kaleta, M. Stange, and R. Bredesen. Development of thin binary and ternary Pd-based alloy membranes for use in hydrogen production. *Journal of Membrane Science*, 383(1-2):124–134, 2011. ISSN 03767388. doi: 10.1016/j.memsci.2011.08.050. URL http://dx.doi.org/10.1016/j.memsci.2011.08.050.

[63] T A Peters, T Kaleta, M Stange, and R Bredesen. Development of ternary Pd–Ag–TM alloy membranes with improved sulphur tolerance. *Journal of Membrane Science*, 429:448–458, 2013. doi: 10.1016/j.memsci.2012.11.062.

[64] Xuezhong He and May Britt Hägg. Hollow fiber carbon membranes: From material to application. *Chemical Engineering Journal*, 215-216:440–448, 2013. ISSN 13858947. doi: 10.1016/j.cej.2012.10.051. URL http://dx.doi.org/10.1016/j.cej.2012.10.051.

[65] T A Peters, M Stange, and R Bredesen. Fabrication of palladium-based membranes by magnetron sputtering. In A Doukelis, K Panopoulos, A Koumanakos, and E Kakaras, editors, *Palladium Membrane Technology for Hydrogen Production, Carbon Capture and Other Application*, pages 25–41. Woodhead Publishing, 2015. doi: 10.1533/9781782422419.1.25.

[66] AM Tarditi, C Imhoff, and F Braun. PdCuAu ternary alloy membranes: Hydrogen permeation properties in the presence of H 2 S. *Journal of Membrane ...*, 479: 246–255, 2014. URL http://www.sciencedirect.com/science/article/pii/S0376738814009338.

[67] T A Peters, M Stange, H Klette, and R Bredesen. High pressure performance of thin Pd–23%Ag/stainless steel composite membranes in water gas shift gas mixtures; influence of dilution, mass transfer and surface effects on

the hydrogen flux. *Journal of Membrane Science*, 316(1-2):119–127, 2008. doi: 10.1016/j.memsci.2007.08.056.

[68] T A Peters, M Stange, P Veenstra, A Nijmeijer, and R Bredesen. The performance of Pd–Ag alloy membrane films under exposure to trace amounts of H2S. *Journal of Membrane Science*, 499:105–115, 2016. doi: 10.1016/j.memsci.2015.10.031.

[69] Nong Xu, Sung Su Kim, Anwu Li, John R Grace, C Jim Lim, and Tony Boyd. Investigation of the influence of tar-containing syngas from biomass gasification on dense Pd and Pd–Ru membranes. *Powder Technology*, 290:132–140, 2016. doi: 10.1016/j.powtec.2015.08.037.

[70] Sean-Thomas B Lundin, Taichiro Yamaguchi, Colin A Wolden, S Ted Oyama, and J Douglas Way. The role (or lack thereof) of nitrogen or ammonia adsorption-induced hydrogen flux inhibition on palladium membrane performance. *Journal of Membrane Science*, 514:65–72, 2016. doi: 10.1016/j.memsci.2016.04.048.

[71] Thu Hoai Nguyen, Shinsuke Mori, and Masaaki Suzuki. Hydrogen permeance and the effect of H2O and CO on the permeability of Pd0.75Ag0.25 membranes under gas-driven permeation and plasma-driven permeation. *Chemical Engineering Journal*, 155(1-2):55–61, 2009. doi: 10.1016/j.cej.2009.06.024.

[72] Bryan D Morreale, Bret H Howard, Osemwengie Iyoha, Robert M Enick, Chen Ling, and David S Sholl. Experimental and Computational Prediction of the Hydrogen Transport Properties of Pd 4 S. *Ind. Eng. Chem. Res.*, 46:6313–6319, 2007.

[73] A Li, W Liang, and R Highes. The effect of carbon monoxide and steam on the hydrogen permeability of a Pd/stainless steel membrane. *Journal of Membrane Science*, 165:135–141, 2000.

[74] Natalie Pomerantz and Ma Yi Hua. Effect of H 2S on the performance and long-term stability of Pd/Cu membranes. *Industrial and Engineering Chemistry Research*, 48(8):4030–4039, 2009. ISSN 08885885. doi: 10.1021/ie801947a.

[75] M Saleh. Interaction of Sulphur Compounds with Palladium. pages 242–250, 1969. ISSN 00147672. doi: 10.1039/TF9706600242.

[76] B. D. Morreale, M. V. Ciocco, B. H. Howard, R. P. Killmeyer, A. V. Cugini, and R. M. Enick. Effect of hydrogen-sulfide on the hydrogen permeance of palladium-copper alloys at elevated temperatures. *Journal of Membrane Science*, 241(2): 219–224, 2004. ISSN 03767388. doi: 10.1016/j.memsci.2004.04.033.

[77] AM Tarditi, C Imhoff, and F Braun. PdCuAu ternary alloy membranes: Hydrogen permeation properties in the presence of H 2 S. *Journal of Membrane science*, 479: 246–255, 2014.

[78] Amanda E Lewis, Hongbin Zhao, Haseeba Syed, Colin A Wolden, and J Douglas Way. PdAu and PdAuAg composite membranes for hydrogen separation from synthetic water-gas shift streams containing hydrogen sulfide. *Journal of Membrane Science*, 465:167–176, 2014. doi: 10.1016/j.memsci.2014.04.022.

[79] CO (US); Shane E. Roark, Boulder, CO (US); Richard MacKay, Lafayette, Michael V. Mundschau Longmont S, and s CO (US). DENSE, LAYERED MEMBRANES FOR HYDROGEN SEPARATION, 2006. ISSN 2004001828.

[80] D.S dos Santos and P.E.V de Miranda. The use of electrochemical hydrogen permeation techniques to detect hydride phase separation in amorphous metallic alloys. *Journal of Non-Crystalline Solids*, 232-234:133–139, 1998. ISSN 00223093. doi: 10.1016/S0022-3093(98)00487-6. URL `http://linkinghub.elsevier.com/retrieve/pii/S0022309398004876`.

[81] Hiroshi Yukawa, Daisuke Yamashita, Shigeyuki Ito, Masahiko Morinaga, and Shu Yamaguchi. Alloying effects on the phase stability of hydrides formed in vanadium alloys. *Materials Transactions*, 43(11):2757–2762, 2002. ISSN 1345-9678. doi: 10.2320/matertrans.43.2757. URL `http://www.jim.or.jp/journal/e/pdf3/43/11/2757.pdf{\%}5Cnpapers2://publication/uuid/3C0A7ADC-9BA8-471E-9CF3-40C116284411{\%}5Cnhttp://joi.jlc.jst.go.jp/JST.JSTAGE/matertrans/43.2757?from=CrossRef`.

[82] Hiroshi Yukawa, Akira Teshima, Daisuke Yamashita, Shigeyuki Ito, Masahiko Morinaga, and Shu Yamaguchi. Alloying effects on the hydriding properties of vanadium at low hydrogen pressures. *Journal of Alloys and Compounds*, 337(1-2):264–268, 2002. ISSN 09258388. doi: 10.1016/S0925-8388(01)01936-3.

[83] Hiroshi Yukawa, Daisuke Yamashita, Shigeyuki Ito, Masahiko Morinaga, and Shu Yamaguchi. Compositional dependence of hydriding properties of vanadium alloys at low hydrogen pressures. *Journal of Alloys and Compounds*, 356-357:45–49, 2003. ISSN 09258388. doi: 10.1016/S0925-8388(03)00099-9.

[84] J. Xu, X. K. Sun, Q. Q. Liu, and W. X. Chen. Hydrogen permeation behavior in IN718 and GH761 superalloys. *Metallurgical and Materials Transactions A*, 25 (3):539–544, 1994. ISSN 10735623. doi: 10.1007/BF02651595.

[85] S Hara, K Sakaki, N Itoh, H.-M. Kimura, K Asami, and A Inoue. An amorphous alloy membrane without noble metals for gaseous hydrogen separation. *Journal of Membrane Science*, 164:289–294, 2000.

[86] Shin-ichi Yamaura, Yoichiro (Fukuda Metal Foil & Powder Co. Ltd.) Shimpo, Hitoshi (Fukuda Metal Foil & Powder Co. Ltd.) Okouchi, Motonori (Fukuda Metal Foil & Powder Co. Ltd.) Nishida, Osamu (Fukuda Metal Foil & Powder Co. Ltd.) Kajita, Hisamichi Kimura, and Akihisa Inoue. Hydrogen Permeation Characteristics of Melt-Spun Ni-Nb-Zr Amorphous Alloy Membranes. *Materials*

Transactions, 42(9):1885–1890, 2001. ISSN 1345-9678. doi: 10.2320/matertrans.42.1885. URL http://ci.nii.ac.jp/naid/130004451634/.

[87] S Hara, K Sakaki, N Itoh, H.-M. Kimura, K Asami, and A Inoue. An amorphous alloy membrane without noble metals for gaseous hydrogen separation. *Journal of Membrane Science*, 164:289–294, 2000.

[88] Shin Ichi Yamaura, Yoichiro Shimpo, Hitoshi Okouchi, Motonori Nishida, Osamu Kajita, and Akihisa Inoue. The effect of additional elements on hydrogen permeation properties of melt-spun Ni-Nb-Zr amorphous alloys. *Nippon Kinzoku Gakkaishi/Journal of the Japan Institute of Metals*, 68(12):1039–1042, 2004. ISSN 00214876. doi: 10.2320/jinstmet.68.1039.

[89] C Nishimura, M Komaki, S Hwang, and M Amano. V-Ni alloy membranes for hydrogen purification. *Journal of Alloys and Compounds*, 330-332:902–906, 2002.

[90] Tetsuya Ozaki, Yi Zhang, Masao Komaki, and Chikashi Nishimura. Preparation of Palladium-coated V and V-15Ni membranes for hydrogen purification by electroless plating technique. *International Journal of Hydrogen Energy*, 28:297–302, 2003.

[91] C. Nishimura, T. Ozaki, M. Komaki, and Y. Zhang. Hydrogen permeation and transmission electron microscope observations of V-Al alloys. *Journal of Alloys and Compounds*, 356-357:295–299, 2003. ISSN 09258388. doi: 10.1016/S0925-8388(02)01273-2.

[92] T. Takano, K. Ishikawa, T. Matsuda, and K. Aoki. Hydrogen Permeation of Eutectic Nb-Zr-Ni Alloy Membranes Containing Primary Phases. *Materials Transactions*, 45(12):3360–3362, 2004. ISSN 13459678. doi: 10.2320/matertrans.45.3360.

[93] Kunihiko Hashi, Kazuhiro Ishikawa, Takeshi Matsuda, and Kiyoshi Aoki. Microstructures and Hydrogen Permeability of Nb-Ti-Ni Alloys with High Resistance to Hydrogen Embrittlement. *Materials Transactions*, 46(5):1026–1031, 2005. ISSN 1345-9678. doi: 10.2320/matertrans.46.1026. URL https://www.jstage.jst.go.jp/article/matertrans/46/5/46{_}5{_}1026/{_}article.

[94] H. Yukawa, T. Nambu, and Y. Matsumoto. Ta-W Alloy for Hydrogen Permeable Membranes. *Materials Transactions*, 52(4):610–613, 2011. ISSN 1347-5320. doi: 10.2320/matertrans.MA201007. URL http://joi.jlc.jst.go.jp/JST.JSTAGE/matertrans/MA201007?from=CrossRef.

[95] Zetian Tao, Litao Yan, Jinli Qiao, Baolin Wang, Lei Zhang, and Jiujun Zhang. A review of advanced proton-conducting materials for hydrogen separation. *Progress in Materials Science*, 74:1–50, 2015. ISSN 00796425. doi: 10.1016/j.pmatsci.2015.04.002. URL http://dx.doi.org/10.1016/j.pmatsci.2015.04.002.

[96] John W. Phair and Richard Donelson. Developments and design of novel (non-palladium-based) metal membranes for hydrogen separation. *Industrial and Engineering Chemistry Research*, 45(16):5657–5674, 2006. ISSN 08885885. doi: 10.1021/ie051333d.

[97] Wen Hui Yuan, Ling Ling Mao, and Li Li. Novel SrCe0.75Zr0.20Tm0.05O3-alpha membrane for hydrogen separation. *Chinese Chemical Letters*, 21(3):369–372, 2010. ISSN 10018417. doi: 10.1016/j.cclet.2009.11.002.

[98] Sonia Escolástico, Cecilia Solís, and José M. Serra. Hydrogen separation and stability study of ceramic membranes based on the system Nd5LnWO12. *International Journal of Hydrogen Energy*, 36(18):11946–11954, 2011. ISSN 03603199. doi: 10.1016/j.ijhydene.2011.06.026.

[99] Sonia Escolástico, Cecilia Solís, Tobias Scherb, Gerhard Schumacher, and Jose M. Serra. Hydrogen separation in La5.5WO11.25-δ membranes. *Journal of Membrane Science*, 444:276–284, 2013. ISSN 03767388. doi: 10.1016/j.memsci.2013.05.005. URL `http://dx.doi.org/10.1016/j.memsci.2013.05.005`.

[100] Sonia Escolástico, Vicente B. Vert, and José M. Serra. Preparation and characterization of nanocrystalline mixed proton-electronic conducting materials based on the system Ln6WO12. *Chemistry of Materials*, 21(14):3079–3089, 2009. ISSN 08974756. doi: 10.1021/cm900067k.

[101] Sonia Escolastico, Janka Seeger, Stefan Roitsch, Mariya Ivanova, Wilhelm A. Meulenberg, and José M. Serra. Enhanced H2 separation through mixed proton-electron conducting membranes based on La5.5W0.8M0.2O 11.25-δ. *ChemSusChem*, 6(8):1523–1532, 2013. ISSN 18645631. doi: 10.1002/cssc.201300091.

[102] Sonia Escolástico, Cecilia Solís, and José M. Serra. Study of hydrogen permeation in (La 5/6Nd 1/6) 5.5WO 12-δ membranes. *Solid State Ionics*, 216:31–35, 2012. ISSN 01672738. doi: 10.1016/j.ssi.2011.11.004. URL `http://dx.doi.org/10.1016/j.ssi.2011.11.004`.

[103] Einar Vøllestad, Camilla K. Vigen, Anna Magrasó, and Reidar Haugsrud. Hydrogen permeation characteristics of La27Mo1.5W3.5O55.5. *Journal of Membrane Science*, 461:81–88, 2014. ISSN 18733123. doi: 10.1016/j.memsci.2014.03.011. URL `http://dx.doi.org/10.1016/j.memsci.2014.03.011`.

[104] Sonia Escolástico, Simona Somacescu, and José M. Serra. Tailoring mixed ionic–electronic conduction in H 2 permeable membranes based on the system Nd 5.5 W 1 x Mo x O 11.25 δ. *J. Mater. Chem. A*, 3(2):719–731, 2015. ISSN 2050-7488. doi: 10.1039/C4TA03699A. URL `http://xlink.rsc.org/?DOI=C4TA03699A`.

[105] Zhiwen Zhu, Wenping Sun, Yingchao Dong, Zhongtao Wang, Zhen Shi, Qingping Zhang, and Wei Liu. Evaluation of hydrogen permeation properties of

Ni–Ba(Zr0.7Pr0.1Y0.2)O3 δ cermet membranes. *International Journal of Hydrogen Energy*, 39(22):11683–11689, 2014. ISSN 03603199. doi: 10.1016/j.ijhydene.2014.05.163. URL http://linkinghub.elsevier.com/retrieve/pii/S0360319914015754.

[106] Zhiwen Zhu, Wenping Sun, Litao Yan, Weifeng Liu, and Wei Liu. Synthesis and hydrogen permeation of Ni–Ba(Zr0.1Ce0.7Y0.2)O3 δ metal–ceramic asymmetric membranes. *International Journal of Hydrogen Energy*, 36(10):6337–6342, 2011. ISSN 03603199. doi: 10.1016/j.ijhydene.2011.02.029. URL http://linkinghub.elsevier.com/retrieve/pii/S0360319911003466.

[107] Jonathan M Polfus, Wen Xing, Marie-Laure Fontaine, Christelle Denonville, Partow P Henriksen, and Rune Bredesen. Hydrogen separation membranes based on dense ceramic composites in the La27W5O55.5-LaCrO3 system. *Journal of Membrane Science*, 479:39–45, 2015. ISSN 03767388. doi: 10.1016/j.memsci.2015.01.027. URL http://dx.doi.org/10.1016/j.memsci.2015.01.027.

[108] S. Escolástico, C. Solís, C. Kjølseth, and J. M. Serra. Outstanding hydrogen permeation through CO ₂ -stable dual-phase ceramic membranes. *Energy Environ. Sci.*, 7(11):3736–3746, 2014. ISSN 1754-5692. doi: 10.1039/C4EE02066A. URL http://xlink.rsc.org/?DOI=C4EE02066A.

[109] Zhiwen Zhu, Wenping Sun, Zhongtao Wang, Jiafeng Cao, Yingchao Dong, and Wei Liu. A high stability Ni-Lainf0.5/infCeinf0.5/infOinf2-δ/inf asymmetrical metal-ceramic membrane for hydrogen separation and generation. *Journal of Power Sources*, 281:417–424, 2015. ISSN 03787753. doi: 10.1016/j.jpowsour.2015.02.005. URL http://dx.doi.org/10.1016/j.jpowsour.2015.02.005.

[110] Shumin Fang, Lei Bi, Litao Yan, and Wenping Sun. CO2 Resistant Hydrogen Permeation Membranes Based on Doped Ceria and Nickel. *Journal of Physical Chemistry C*, pages 10986–10991, 2010. ISSN 1932-7447. doi: 10.1021/jp102271v. URL http://pubs.acs.org/doi/abs/10.1021/jp102271v.

[111] Litao Yan, Wenping Sun, Lei Bi, Shumin Fang, Zetian Tao, and Wei Liu. Effect of Sm-doping on the hydrogen permeation of Ni-La2Ce2O7 mixed protonic-electronic conductor. *International Journal of Hydrogen Energy*, 35(10):4508–4511, 2010. ISSN 03603199. doi: 10.1016/j.ijhydene.2010.02.134. URL http://dx.doi.org/10.1016/j.ijhydene.2010.02.134.

[112] Jay Kniep and Y. S. Lin. Effect of zirconium doping on hydrogen permeation through strontium cerate membranes. *Industrial and Engineering Chemistry Research*, 49(6):2768–2774, 2010. ISSN 08885885. doi: 10.1021/ie9015182.

[113] Tak keun Oh, Heesung Yoon, and E. D. Wachsman. Effect of Eu dopant concentration in SrCe1 - xEuxO3 - ?? on ambipolar conductivity. *Solid State Ionics*, 180 (23-25):1233–1239, 2009. ISSN 01672738. doi: 10.1016/j.ssi.2009.07.001.

[114] Wei Liu, Victor G. Ruiz, Guo Xu Zhang, Biswajit Santra, Xinguo Ren, Matthias Scheffler, and Alexandre Tkatchenko. Structure and energetics of benzene adsorbed on transition-metal surfaces: Density-functional theory with van der Waals interactions including collective substrate response. *New Journal of Physics*, 15 (111), 2013. ISSN 13672630. doi: 10.1088/1367-2630/15/5/053046.

[115] Jian Song, Liping Li, Xiaoyao Tan, and K. Li. BaCe0.85Tb0.05Co0.1O3-?? perovskite hollow fibre membranes for hydrogen/oxygen permeation. *International Journal of Hydrogen Energy*, 38(19):7904–7912, 2013. ISSN 03603199. doi: 10.1016/j.ijhydene.2013.04.104.

[116] Shumin Fang, Kyle Brinkman, and Fanglin Chen. Unprecedented CO ₂ -Promoted Hydrogen Permeation in Ni-BaZr _{0.1} Ce _{0.7} Y _{0.1} Yb _{0.1} O _{3 δ} Membrane. *ACS Applied Materials & Interfaces*, 6(1):725–730, 2014. ISSN 1944-8244. doi: 10.1021/am405169d. URL `http://pubs.acs.org/doi/abs/10.1021/am405169d`.

[117] Shumin Fang, Kyle S. Brinkman, and Fanglin Chen. Hydrogen permeability and chemical stability of Ni-BaZr0.1Ce0.7Y0.1Yb0.1O3-δ membrane in concentrated H2O and CO2. *Journal of Membrane Science*, 467:85–92, 2014. ISSN 18733123. doi: 10.1016/j.memsci.2014.05.008. URL `http://dx.doi.org/10.1016/j.memsci.2014.05.008`.

[118] Xihan Tan, Xiaoyao Tan, Naitao Yang, Bo Meng, Kun Zhang, and Shaomin Liu. High performance BaCe0.8Y0.2O3-A (BCY) hollow fibre membranes for hydrogen permeation. *Ceramics International*, 40(2):3131–3138, 2014. ISSN 02728842. doi: 10.1016/j.ceramint.2013.09.132.

[119] Vanesa Gil, Jonas Gurauskis, Christian Kjølseth, Kjell Wiik, and Mari-Ann Einarsrud. Hydrogen permeation in asymmetric La28 xW4 + xO54 + 3x/2 membranes. *International Journal of Hydrogen Energy*, 38(7):3087–3091, 2013. ISSN 03603199. doi: 10.1016/j.ijhydene.2012.12.105. URL `http://linkinghub.elsevier.com/retrieve/pii/S0360319912028406`.

[120] Camilla K. Vigen and Reidar Haugsrud. Hydrogen flux in La0.87Sr0.13CrO3-δ. *Journal of Membrane Science*, 468:317–323, 2014. ISSN 18733123. doi: 10.1016/j.memsci.2014.06.012.

[121] Jian Song, Bo Meng, Xiaoyao Tan, and Shaomin Liu. Surface-modified proton conducting perovskite hollow fibre membranes by Pd-coating for enhanced hydrogen permeation. *International Journal of Hydrogen Energy*, 40(18):6118–6127, 2015. ISSN 03603199. doi: 10.1016/j.ijhydene.2015.03.057. URL `http://dx.doi.org/10.1016/j.ijhydene.2015.03.057`.

[122] Jian Song, Jian Kang, Xiaoyao Tan, Bo Meng, and Shaomin Liu. Proton conducting perovskite hollow fibre membranes with surface catalytic modification for

enhanced hydrogen separation. *Journal of the European Ceramic Society*, 36(7): 1669–1677, 2015. ISSN 1873619X. doi: 10.1016/j.jeurceramsoc.2016.01.006. URL http://dx.doi.org/10.1016/j.jeurceramsoc.2016.01.006.

[123] Ivan P. Mardilovich, Erik Engwall, and Yi Hua Ma. Dependence of hydrogen flux on the pore size and plating surface topology of asymmetric Pd-porous stainless steel membranes. *Desalination*, 144(1-3):85–89, 2002. ISSN 00119164. doi: 10.1016/S0011-9164(02)00293-X.

[124] E.-U. Schlünder, J. Yang, and A. Seidel-Morgenstern. Competitive diffusion and adsorption in vycor glass membranes—a lumped parameter approach. *Catalysis Today*, 118(1):113 – 120, 2006. ISSN 0920-5861. doi: https://doi.org/10.1016/j.cattod.2005.11.094. URL http://www.sciencedirect.com/science/article/pii/S0920586106003488. Catalysis in Membrane Reactors.

[125] Shigeyuki Uemiya, Noboru Sato, Hiroshi Ando, Yukinori Kude, Takeshi Matsuda, and Eiichi Kikuchi. Separation of hydrogen through palladium thin film supported on a porous glass tube. *Journal of Membrane Science*, 56(3):303 – 313, 1991. ISSN 0376-7388. doi: https://doi.org/10.1016/S0376-7388(00)83040-9. URL http://www.sciencedirect.com/science/article/pii/S0376738800830409.

[126] S. Mukherjee, M.K. Hatalis, and M.V. Kothare. Water gas shift reaction in a glass microreactor. *Catalysis Today*, 120(1):107 – 120, 2007. ISSN 0920-5861. doi: https://doi.org/10.1016/j.cattod.2006.07.007. URL http://www.sciencedirect.com/science/article/pii/S092058610600438X. The Novel Compact Catalytic Reactor.

[127] Hideko Hayashi, Tetsuya Saitou, Naotaka Maruyama, Hideaki Inaba, Katsuyuki Kawamura, and Masashi Mori. Thermal expansion coefficient of yttria stabilized zirconia for various yttria contents. *Solid State Ionics*, 176(5-6):613–619, 2005. ISSN 01672738. doi: 10.1016/j.ssi.2004.08.021.

[128] Samhun Yun and S Ted Oyama. Correlations in palladium membranes for hydrogen separation: A review. *Journal of Membrane Science*, 375(1-2):28–45, 2011. doi: 10.1016/j.memsci.2011.03.057.

[129] W P Wang, S Thomas, X L Zhang, X L Pan, W S Yang, and G X Xiong. H2/N2 gaseous mixture separation in dense Pd/α-Al2O3 hollow fiber membranes: Experimental and simulation studies. *Separation and Purification Technology*, 52(1): 177–185, 2006. doi: 10.1016/j.seppur.2006.04.007.

[130] E David and J Kopac. Devlopment of palladium/ceramic membranes for hydrogen separation. *International Journal of Hydrogen Energy*, 36(7):4498–4506, 2011. doi: 10.1016/j.ijhydene.2010.12.032.

[131] Yan Huang and Roland Dittmeyer. Preparation of thin palladium membranes on a porous support with rough surface. *Journal of Membrane Science*, 302(1):160 – 170, 2007. ISSN 0376-7388. doi: https://doi.org/10.1016/j.memsci.2007.06.040. URL http://www.sciencedirect.com/science/article/pii/S0376738807004358.

[132] Zhong Yan Li, Hideaki Maeda, Katsuki Kusakabe, Shigeharu Morooka, Hiroshi Anzai, and Shigeo Akiyama. Preparation of palladium-silver alloy membranes for hydrogen separation by the spray pyrolysis method. *Journal of Membrane Science*, 78(3):247 – 254, 1993. ISSN 0376-7388. doi: https://doi.org/10.1016/0376-7388(93)80004-H. URL http://www.sciencedirect.com/science/article/pii/037673889380004H.

[133] Angelo Basile, Fausto Gallucci, and Silvano Tosti. Synthesis, Characterization, and Applications of Palladium Membranes. 13:255–323, 2008. doi: 10.1016/s0927-5193(07)13008-4.

[134] T A Peters, M Stange, and R Bredesen. Fabrication of palladium-based membranes by magnetron sputtering. In A Doukelis, K Panopoulos, A Koumanakos, and E Kakaras, editors, *Palladium Membrane Technology for Hydrogen Production, Carbon Capture and Other Application*, pages 25–41. Woodhead Publishing, 2015. doi: 10.1533/9781782422419.1.25.

[135] George Xomeritakis and Y. S. Lin. Fabrication of thin metallic membranes by MOCVD and sputtering. *Journal of Membrane Science*, 133(2):217–230, 1997. ISSN 03767388. doi: 10.1016/S0376-7388(97)00084-7.

[136] B. McCool, G. Xomeritakis, and Y. S. Lin. Composition control and hydrogen permeation characteristics of sputter deposited palladium-silver membranes. *Journal of Membrane Science*, 161(1-2):67–76, 1999. ISSN 03767388. doi: 10.1016/S0376-7388(99)00087-3.

[137] Jos T. F. Keurentjes, Frank C. Gielens, H. D. Tong, C. J. M. van Rijn, and Marius a. G. Vorstman. High-Flux Palladium Membranes Based on Microsystem Technology. *Industrial & Engineering Chemistry Research*, 43(16):4768–4772, 2004. ISSN 0888-5885. doi: 10.1021/ie0341202. URL http://pubs.acs.org/doi/abs/10.1021/ie0341202.

[138] Kenneth J. Bryden and Jackie Y. Ying. Nanostructured palladium membrane synthesis by magnetron sputtering. *Materials Science and Engineering A*, 204 (1-2):140–145, 1995. ISSN 09215093. doi: 10.1016/0921-5093(95)09950-6.

[139] M J den Exter. The use of electroless plating as a deposition technology in the fabrication of palladium-based membranes. In A Doukelis, K Panopoulos, A Koumanakos, and E Kakaras, editors, *Palladium Membrane Technology for Hydrogen Production, Carbon Capture and Other Application*, pages 43–67. Woodhead Publishing, 2015. doi: 10.1533/9781782422419.1.43.

[140] E Kikuchi and S Uemiya. Preparation of supported thin palladium-silver alloy membranes and their characteristics for hydrogen separation. *Gas Separation and Purification*, 5, 1991.

[141] David S. Sholl. Using density functional theory to study hydrogen diffusion in metals: A brief overview. *Journal of Alloys and Compounds*, 446-447:462 – 468, 2007. ISSN 0925-8388. doi: https://doi.org/10.1016/j.jallcom.2006.10.136. URL http://www.sciencedirect.com/science/article/pii/S0925838806017439. Proceedings of the International Symposium on Metal-Hydrogen Systems, Fundamentals and Applications (MH2006).

[142] Kelly M. Nicholson, Nita Chandrasekhar, and David S. Sholl. Powered by dft: Screening methods that accelerate materials development for hydrogen in metals applications. *Accounts of Chemical Research*, 47(11):3275–3283, 2014. doi: 10.1021/ar500018b. URL https://doi.org/10.1021/ar500018b. PMID: 24937509.

[143] *DFT Calculations for Simple Solids*, chapter 2, pages 35–48. John Wiley & Sons, Ltd, 2009. ISBN 9780470447710. doi: 10.1002/9780470447710.ch2. URL https://onlinelibrary.wiley.com/doi/abs/10.1002/9780470447710.ch2.

[144] *DFT Calculations for Surfaces of Solids*, chapter 4, pages 83–112. John Wiley & Sons, Ltd, 2009. ISBN 9780470447710. doi: 10.1002/9780470447710.ch4. URL https://onlinelibrary.wiley.com/doi/abs/10.1002/9780470447710.ch4.

[145] David Alique, David Martinez-Diaz, Raul Sanz, and Jose Calles. Review of supported pd-based membranes preparation by electroless plating for ultra-pure hydrogen production. *Membranes*, 8(1):5, Jan 2018. ISSN 2077-0375. doi: 10.3390/membranes8010005. URL http://dx.doi.org/10.3390/membranes8010005.

[146] Zhenhua Zeng, Juarez Da Silva, Hui-Qiu Deng, and Wei-Xue Li. Density functional theory study of the energetics, electronic structure, and core-level shifts of no adsorption on the pt(111) surface. *Phys. Rev. B*, 79, 05 2009. doi: 10.1103/PhysRevB.79.205413.

[147] *What is Density Functional Theory?*, chapter 1, pages 1–33. John Wiley & Sons, Ltd, 2009. ISBN 9780470447710. doi: 10.1002/9780470447710.ch1. URL https://onlinelibrary.wiley.com/doi/abs/10.1002/9780470447710.ch1.

[148] O. M. Løvvik and R. A. Olsen. Density functional calculations of hydrogen adsorption on palladium–silver alloy surfaces. *The Journal of Chemical Physics*, 118 (7):3268–3276, 2003. doi: 10.1063/1.1536955. URL https://doi.org/10.1063/1.1536955.

[149] Ekin Ozdogan and Jennifer Wilcox. Investigation of h2 and h2s adsorption on niobium- and copper-doped palladium surfaces. *The Journal of Physical Chemistry B*, 114(40):12851–12858, 2010. doi: 10.1021/jp105469c. URL https://doi.org/10.1021/jp105469c. PMID: 20845969.

[150] Jeffrey A. Herron, Scott Tonelli, and Manos Mavrikakis. Atomic and molecular adsorption on pd(111). *Surface Science*, 606(21):1670 – 1679, 2012. ISSN 0039-6028. doi: https://doi.org/10.1016/j.susc.2012.07.003. URL http://www.sciencedirect.com/science/article/pii/S0039602812002245.

[151] Preeti Kamakoti, Bryan D. Morreale, Michael V. Ciocco, Bret H. Howard, Richard P. Killmeyer, Anthony V. Cugini, and David S. Sholl. Prediction of hydrogen flux through sulfur-tolerant binary alloy membranes. *Science*, 307 (5709):569–573, 2005. ISSN 0036-8075. doi: 10.1126/science.1107041. URL https://science.sciencemag.org/content/307/5709/569.

[152] Preeti Kamakoti and David S. Sholl. A comparison of hydrogen diffusivities in pd and cupd alloys using density functional theory. *Journal of Membrane Science*, 225(1):145 – 154, 2003. ISSN 0376-7388. doi: https://doi.org/10.1016/j.memsci.2003.07.008. URL http://www.sciencedirect.com/science/article/pii/S0376738803003831.

[153] Preeti Kamakoti and David S. Sholl. Ab initio lattice-gas modeling of interstitial hydrogen diffusion in cupd alloys. *Phys. Rev. B*, 71:014301, Jan 2005. doi: 10.1103/PhysRevB.71.014301. URL https://link.aps.org/doi/10.1103/PhysRevB.71.014301.

[154] Chandrashekhar G. Sonwane, Jennifer Wilcox, and Yi Hua Ma. Achieving optimum hydrogen permeability in pdag and pdau alloys. *The Journal of Chemical Physics*, 125(18):184714, 2006. doi: 10.1063/1.2387166. URL https://doi.org/10.1063/1.2387166.

[155] Chandrashekhar G. Sonwane, Jennifer Wilcox, and Yi Hua Ma. Solubility of hydrogen in pdag and pdau binary alloys using density functional theory. *The Journal of Physical Chemistry B*, 110(48):24549–24558, 2006. doi: 10.1021/jp064507t. URL https://doi.org/10.1021/jp064507t. PMID: 17134214.

[156] Shucheng Xu, Parveen Sood, M. L. Liu, and Angelo Bongiorno. First-principles study of hydrogen permeation in palladium-gold alloys. *Applied Physics Letters*, 99(18):181901, 2011. doi: 10.1063/1.3656739. URL https://doi.org/10.1063/1.3656739.

[157] Preeti Kamakoti and David Sholl. Towards first principles-based identification of ternary alloys for hydrogen purification membranes. *Journal of Membrane Science - J MEMBRANE SCI*, 279:94–99, 08 2006. doi: 10.1016/j.memsci.2005.11.035.

[158] Lymarie Semidey-Flecha, Chen Ling, and David S. Sholl. Detailed first-principles models of hydrogen permeation through pdcu-based ternary alloys. *Journal of Membrane Science*, 362(1):384 – 392, 2010. ISSN 0376-7388. doi: https://doi.org/10.1016/j.memsci.2010.06.063. URL http://www.sciencedirect.com/science/article/pii/S0376738810005302.

[159] Chen Ling, Lymarie Semidey-Flecha, and David S. Sholl. First-principles screening of pdcuag ternary alloys as h2 purification membranes. *Journal of Membrane Science*, 371(1):189 – 196, 2011. ISSN 0376-7388. doi: https://doi.org/10.1016/j.memsci.2011.01.030. URL http://www.sciencedirect.com/science/article/pii/S0376738811000494.